

Behavioral Abnormalities and Circuit Defects in the Basal Ganglia of a Mouse Model of 16p11.2 Deletion Syndrome

Thomas Portmann,^{1,2} Mu Yang,^{3,13,14} Rong Mao,^{1,2,13} Georgia Panagiotakos,^{1,2,4,13} Jacob Ellegood,⁵ Gul Dolen,⁶ Patrick L. Bader,^{2,7} Brad A. Grueter,^{2,8} Carleton Goold,^{1,2} Elaine Fisher,^{1,2} Katherine Clifford,^{1,2} Pavitra Rengarajan,^{1,2} David Kalikhman,³ Darren Loureiro,³ Nay L. Saw,⁹ Zhou Zhengqui,⁹ Michael A. Miller,⁹ Jason P. Lerch,^{5,10} R. Mark Henkelman,^{5,10} Mehrdad Shamloo,^{2,9,11} Robert C. Malenka,^{2,8} Jacqueline N. Crawley,^{3,14} and Ricardo E. Dolmetsch^{1,12,*}

¹Department of Neurobiology, Stanford University, Stanford, CA 94305-5345, USA

²School of Medicine, Stanford University, Stanford, CA 94305-5345, USA

³Laboratory of Behavioral Neuroscience, National Institute of Mental Health, Bethesda, MD 20892-9663, USA

⁴Neurosciences Program, Stanford University, Stanford, CA 94305-5345, USA

⁵Mouse Imaging Centre (MICe), Hospital for Sick Children, Toronto, ON M5T 3H7, Canada

⁶Department of Neuroscience, Brain Science Institute, Johns Hopkins University, Baltimore, MD 21205, USA

⁷Department of Molecular and Cellular Physiology, Stanford University, Stanford, CA 94305-5345, USA

⁸Nancy Pritzker Laboratory, Department of Psychiatry and Behavioral Sciences, Stanford University, Stanford, CA 94305-5345, USA

⁹Stanford Behavioral and Functional Neuroscience Laboratory, Stanford, CA 94305-5345, USA

¹⁰Department of Medical Biophysics, University of Toronto, Toronto, ON M5G 1L7, Canada

¹¹Stanford Institute for Neuro-Innovation and Translational Neurosciences, Stanford, CA 94305-5345, USA

¹²Novartis Institutes for Biomedical Research, Cambridge, MA 02139, USA

¹³These authors contributed equally to this work

¹⁴Present address: MIND Institute and Department of Psychiatry and Behavioral Sciences, UC Davis School of Medicine, Sacramento, CA 95817, USA

*Correspondence: ricardo.dolmetsch@novartis.com

<http://dx.doi.org/10.1016/j.celrep.2014.03.036>

This is an open access article under the CC BY-NC-ND license (<http://creativecommons.org/licenses/by-nc-nd/3.0/>).

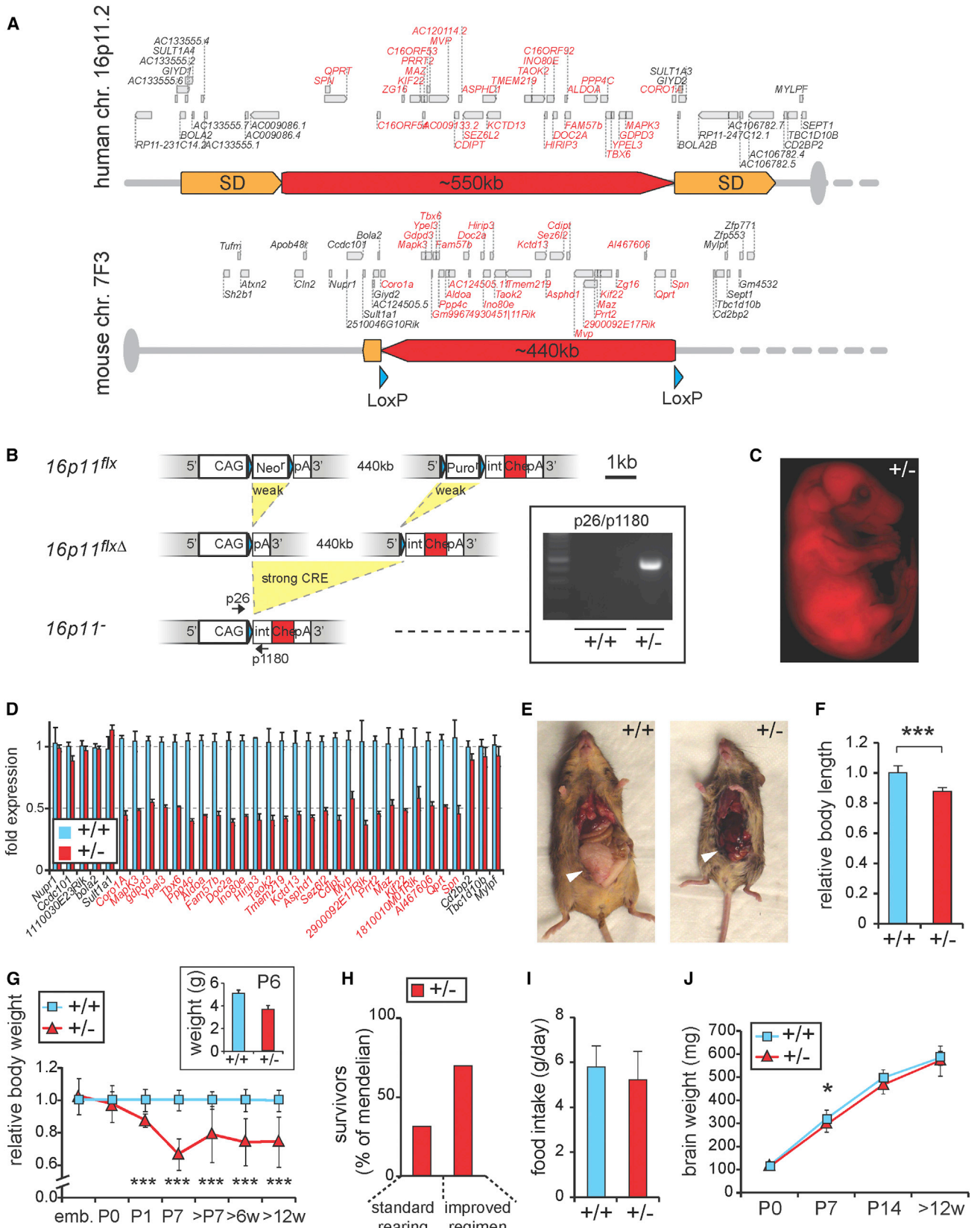
SUMMARY

A deletion on human chromosome 16p11.2 is associated with autism spectrum disorders. We deleted the syntenic region on mouse chromosome 7F3. MRI and high-throughput single-cell transcriptomics revealed anatomical and cellular abnormalities, particularly in cortex and striatum of juvenile mutant mice (*16p11^{+/-}*). We found elevated numbers of striatal medium spiny neurons (MSNs) expressing the dopamine D2 receptor (*Drd2⁺*) and fewer dopamine-sensitive (*Drd1⁺*) neurons in deep layers of cortex. Electrophysiological recordings of *Drd2⁺* MSN revealed synaptic defects, suggesting abnormal basal ganglia circuitry function in *16p11^{+/-}* mice. This is further supported by behavioral experiments showing hyperactivity, circling, and deficits in movement control. Strikingly, *16p11^{+/-}* mice showed a complete lack of habituation reminiscent of what is observed in some autistic individuals. Our findings unveil a fundamental role of genes affected by the 16p11.2 deletion in establishing the basal ganglia circuitry and provide insights in the pathophysiology of autism.

INTRODUCTION

Autism spectrum disorders (ASD) are characterized by social deficits, language impairments, and stereotyped behaviors manifested in early childhood (Geschwind and Levitt, 2007). Epidemiological studies have reported a dramatic increase in the prevalence of ASD (Fombonne, 2003), now estimated to affect more than 1 in 100 children (Baron-Cohen et al., 2009). A number of genomic loci have been associated with increased risk for ASD (Abrahams and Geschwind, 2008; Persico and Bourgeron, 2006). A copy number variation (CNV) on human chromosome 16p11.2 is among the most common genetic variations found in ASD (Weiss et al., 2008). Patients with this deletion display motor deficits, speech/language delay, and cognitive impairments, accompanied by ASD, attention deficit hyperactivity disorder (ADHD), seizures, and hearing disorders (Bijlsma et al., 2009; Fernandez et al., 2010; Shinawi et al., 2010). Conversely, a duplication of 16p11.2 is associated with schizophrenia (McCarthy et al., 2009).

The most common deletion in the 16p11.2 locus associated with ASD causes loss of 550 kb of genomic DNA and haploinsufficiency of 26 genes. Knockdown and overexpression studies have attempted to model these gene dosage changes, implicating two genes, *Kctd13* and *Taok2*, in altered brain size and neurite morphogenesis, respectively (de Anda et al., 2012; Golzio et al., 2012). However, it is not known whether knockdown-mediated dosage changes accurately model loss of a



(legend on next page)

single allele for each of these genes. A 16p11.2 CNV adult mouse model was recently reported to display activity-related behavioral deficits and subtle morphological changes in the ventral midbrain (Horev et al., 2011). Nevertheless, the defects in brain development in the context of the 16p11.2 deletion that may underlie behavioral abnormalities in patients remain unclear.

Neural circuits modulated by the neurotransmitter dopamine (DA) play an important role in motor, cognitive, and emotional control (for review, see DeLong and Wichmann, 2009). DA neurons in the ventral midbrain send projections to the striatum and cortex. The striatum contains DA-sensitive medium spiny neurons (MSNs) and is the entry point of the basal ganglia (BG) circuitry, which plays a major role in motor control, motivation, and attention. MSNs that express either dopamine D1 (*Drd1*⁺) or D2 (*Drd2*⁺) receptors act antagonistically through the direct (striatonigral) and indirect (striatopallidal) pathways, respectively (Kravitz et al., 2012). DA also modulates the activity of *Drd1*⁺ neurons in deeper layers of cortex. The role of these cells in regulating behavior has not been studied extensively. Some cortical *Drd1*⁺ cells project back to striatal MSNs, providing important top-down control of movements, motivation, and attention. These cells have also been proposed to play a role in gain control of cortical inputs, as well as in mediating the effects of DA on learning and memory (Olsen et al., 2012; Seong and Carter, 2012; Thurley et al., 2008). The circuits modulated by DA play an important role in the pathophysiology of several neurologic and psychiatric diseases. ADHD is clinically treated with drugs altering DA levels, like dexamphetamine and methylphenidate, suggesting DA misregulation as a key element in the etiology of this disorder. In contrast, agents like risperidone that block D2 receptors (D2Rs) are used both to control irritability in ASD and as antipsychotics in schizophrenia, implicating these circuits in the biogenesis of these disorders. Although DA-modulated circuits are strongly implicated in schizophrenia, ADHD, and ASD, the underlying anatomical or molecular defects in patients are largely unknown.

We generated a mouse model for the 16p11.2 deletion. Using high-throughput multiplex single-cell gene expression analysis (sc-qPCR) to identify cell-type-specific deficits across the developing mouse brain, we found that 16p11.2 heterozygous (*16p11*^{+/-}) mice have increased numbers of *Drd2*⁺ striatal

MSNs, as well as fewer *Drd1*⁺ neurons in cortex. MRI revealed anatomical defects of BG nuclei, direct targets of BG output structures, and several cortical regions. Electrophysiological recordings suggested synaptic alterations in *Drd2*⁺ MSNs. Finally, extensive behavioral analyses carried out by two independent laboratories revealed that *16p11*^{+/-} mice exhibit normal social behavior but show hyperactivity and deficits in movement control, hearing, and habituation to familiarity. Taken together, our findings suggest that BG circuitry and DA signaling play a critical role in the defects of the 16p11.2 deletion, and more generally, in the pathophysiology of ADHD and ASD.

RESULTS

A Mouse Model for the Human Chromosome 16p11.2 Microdeletion

The chromosome 16p11.2 CNV encompasses 26 genes (the *16p11* genes) that are highly conserved on mouse chromosome 7F3 (Figure 1A). To generate a mouse model of the 16p11.2 deletion, we introduced LoxP sites flanking the genes deleted in human patients (Figures 1B, S1A, and S1B). The targeting strategy also included an *mCherry* reporter gene coupled to deletion of the region. Successful targeting of mouse embryonic stem cells (mESCs) was verified by Southern blotting and PCR (Figures S1C–S1I; Table S1). The modified mESCs were injected into blastocysts, implanted into pseudopregnant female mice, and chimeric offspring were subsequently bred to (1) C57BL/6N females to produce heterozygous floxed (*16p11*^{flx/+}) mice and (2) *HPRT-Cre* transgenic females (Tang et al., 2002) to produce mice lacking one copy of the *16p11* genes (*16p11*^{+/-}). Heterozygous deletion was confirmed by PCR genotyping, as well as mCherry fluorescence (Figures 1B, inset, and 1C). Quantitative real-time RT-PCR (qPCR) analysis of neonate brain RNA showed a global reduction in transcription of 40%–60% for the *16p11* genes upon loss of one copy (Figure 1D). F1 and further generations of *16p11*^{+/-} male mice were consequently backbred to C57BL/6N females.

16p11^{+/-} mice were born at Mendelian ratios. As adults, they showed a 12.2% reduction in average body length ($p = 5.09 \times 10^{-7}$; Figures 1E and 1F), a reduction in the accumulation of abdominal fat pads, and significantly reduced body weight

Figure 1. A Mouse Model for the Human 16p11.2 Microdeletion

- (A) Top: the region on human chromosome 16p11.2 is flanked by segmental duplications (SD), which likely mediate CNVs of the locus by nonhomologous recombination. Bottom: the syntenic region on mouse chromosome 7F3, in which LoxP sites (blue arrowheads) were inserted at positions indicated.
- (B) Sequential recombination steps yield deletion of 440 kb containing the mouse *16p11* genes. pA, poly A; int, intron; CAG, chicken β -actin enhanced CMV promoter; *Neo*^r and *Puro*^r, neomycin and puromycin resistance cassettes; STOP, translational stop codon; *Che*, *mCherry*. Scale bar, 1 kb. Inset, Genotyping of F1 offspring from floxed (*16p11*^{flx/+}) chimeras and *HPRT-Cre*^{tg/+} females shows germline transmission. Arrows in scheme show PCR primer positions.
- (C) Red fluorescence in E16.5 *16p11*^{+/-} embryo confirms *mCherry* expression and deletion of *16p11* genes.
- (D) At birth (P0): qPCR analysis shows global downregulation of *16p11* genes (red) in the brain upon deletion of one allele, whereas neighboring genes are unaffected.
- (E) Adult animals (4 months): *16p11*^{+/-} females lack abdominal fat pads (white arrowheads) typical for this age.
- (F) Adult animals (3 months): relative body length ($n = 12$).
- (G) Relative body weight ($n \geq 6$ per time point) across development normalized to the average of gender-matched wild-type littermates. Inset: independent analysis of body weight performed at NIMH at P6.
- (H) At 6 weeks of age: increased juvenile mortality of *16p11*^{+/-} mice is rescued by improved nutritional regimen and alleviated sibling competition.
- (I) Adult animals (3 months): food intake is comparable between *16p11*^{+/-} and wild-type animals.
- (J) Postnatal developmental trajectory of brain weight as a measure for global brain growth ($n \geq 6$).
- Data are mean \pm SEM. * $p < 0.05$, ** $p < 0.01$, and *** $p < 0.001$. Inset in (G), NIMH.

starting at early postnatal age (Figure 1G). A small number of $16p11^{+/-}$ animals recovered to nearly normal body weight in adulthood. Severely affected mice were runty and died within the first postnatal weeks (Figure 1H), resulting in lower-than-Mendelian ratios of survivors past the age of tagging (typically 6 weeks). An improved nutritional regimen and alleviated competition by wild-type siblings rescued $16p11^{+/-}$ pup viability to 60% of Mendelian expectation (Figure 1H; Supplemental Experimental Procedures). Food intake in adult $16p11^{+/-}$ animals was normal (Figure 1I). $16p11^{+/-}$ pups appeared hyperactive and displayed severe deficits in motor coordination including tumbling and tremor (Movie S1). These findings were replicated and quantified in adult animals as described below. In contrast to the decreased body size, the brain weight of $16p11^{+/-}$ mice was indistinguishable from controls (Figure 1J) throughout development, with the exception of 1-week-old (P7) pups, in which the brain weight was mildly reduced ($p < 0.05$).

MRI and Diffusion Tensor Image Analyses of Juvenile Brains

MRI in P7 mice revealed decreased brain volume throughout the $16p11^{+/-}$ brain (total -13.0% ; Figures 2A–2C and 2E), consistent with decreased brain weight at this age. The relative volume (normalized to total brain volume) of several structures revealed more complex abnormalities, particularly in the BG, direct targets of BG output structures (thalamus and superior colliculus), and major afferent regions to the BG (cortex and thalamus). In the BG, the dorsal striatum showed significant expansion in the dorsofrontal direction and reduction at ventrocaudal areas, although the relative volume was unchanged (Figure 2A; $+0.42\%$, n.s.). The relative volume of the nucleus accumbens (NAc) was increased by 4.83% in $16p11^{+/-}$ pups compared to wild-type (Figure 2B; $q < 0.01$). The globus pallidus (GP), a major target of striatal afferents, showed a 2.79% increase in relative volume in $16p11^{+/-}$ pups (Figure 2C; $q < 0.01$), suggesting a potential link between striatal and pallidal abnormalities. These changes in the BG were accompanied by major structural defects in brain regions projecting to striatum. Abnormalities in the $16p11^{+/-}$ cortex encompassed increased thickness in medial areas including motor cortices (Figure 2D). In contrast, lateral, and ventral areas, including sensory (e.g., primary auditory cortex) and insular cortices, showed significant reduction in thickness. Mesodiencephalic structures were increased in size, including the thalamus ($+9.6\%$, $q < 0.01$), hypothalamus ($+4.2\%$, $q < 0.01$), and superior and inferior colliculi ($+5.9\%$ and $+11.7\%$ respectively, both with $q < 0.01$). In conclusion, MRI data suggest major structural abnormalities in the early postnatal $16p11^{+/-}$ brain, affecting primarily the BG, cortex, and regions of the mesodiencephalon, which receive projections from BG output structures.

Single-Cell Gene Expression Analysis

The complex anatomical defects in the brain of juvenile $16p11^{+/-}$ mice suggested defects in specific cell populations. We previously established multiplex sc-qPCR using nanofluidic array technology as a powerful tool to study the cellular composition of heterogeneous cell populations in vitro (Pasca et al., 2011; Yoo et al., 2011). Here, we adapted the method to study the

composition of cells in defined anatomical regions of the brain: cerebral cortex, hippocampus, subpallium (including striatum, NAc, GP, and amygdala), and mesodiencephalon (Figure 3A). To ensure that our findings would not reflect secondary consequences of the early postnatal weight loss in $16p11^{+/-}$ pups, we performed this analysis in neonate mice (P0), which were morphologically indistinguishable from wild-type. After tissue dissociation, single cells were sorted into 96-well PCR plates using fluorescence activated cell sorting (FACS). Expression of 190 genes (Table S2) was measured in each of more than 2,000 single cells. We selected genes that by virtue of their expression pattern best distinguished specific neural cell types, encoding transcription factors, neurotransmitter receptors, synthetic enzymes, and guidance molecules. In addition, we included the $16p11$ genes.

sc-qPCR data showed a lognormal distribution (Figure S2A) and high variability across cells (average SD: 1.73 PCR cycles, average range: 7.93 PCR cycles; $n = 172$ genes; $n > 2,000$ cells, Figure S2B) consistent with previous studies suggesting that mRNA levels in a single cell are largely a function of the bursting kinetics of gene transcription (Bengtsson et al., 2005; Suter et al., 2011). To eliminate this source of variability data were binarized and a Fisher's exact test p value (p_{FET}) was calculated for the observed coexpression of a gene with every other gene based on the expected coexpression frequency if they were randomly assigned to cells. The logarithm of these p values ($\log[p_{FET}]$) was supplied with an algebraic sign, in order to recover information about increased coexpression or mutual exclusiveness that was lost in the process of assessing the significance of the deviation from the expected coexpression of genes (Experimental Procedures; Supplemental Experimental Procedures). The diagonal symmetric coexpression matrix was then subjected to unsupervised clustering (Figures 3 and S2I). The resulting gene clusters identified major neuronal subtypes in the examined brain regions. By example, the subpallium (Figure 3B) included GABAergic neurons, striatal MSNs, striatopallidal MSNs, striatal interneurons, neurons of the amygdala, lateral migratory stream, GP, and lateral ventricular wall progenitors (Arlotta et al., 2008; Ding et al., 2012; Marin et al., 2000; Nóbrega-Pereira et al., 2010). In the cortex (Figure 3C), we found gene clusters that distinguish progenitor populations, cortical interneurons, and distinct groups of cortical excitatory neurons. Among these are deeper layer excitatory neurons that are born earliest during corticogenesis and already express mature markers indicating synaptogenesis, upper layer excitatory neurons generated late in embryogenesis, and ventricular zone (VZ) progenitors, which in the neonate also start to express glial progenitor markers (Arlotta et al., 2005; Chen et al., 2008; Lai et al., 2008; Molnár and Cheung, 2006; Sasaki et al., 2008; Takemoto et al., 2011). This analysis strategy therefore identified gene clusters correlating with specific cell types previously described using other methods in vivo.

Altered DA Signaling in the Neonate $16p11^{+/-}$ Brain

Using these tools, we found that $16p11^{+/-}$ and wild-type mice have highly similar cell-type-specific gene clusters, suggesting that the mutation does not lead to the generation of ectopic cell types or to complete loss of existing ones (Figures 3D and

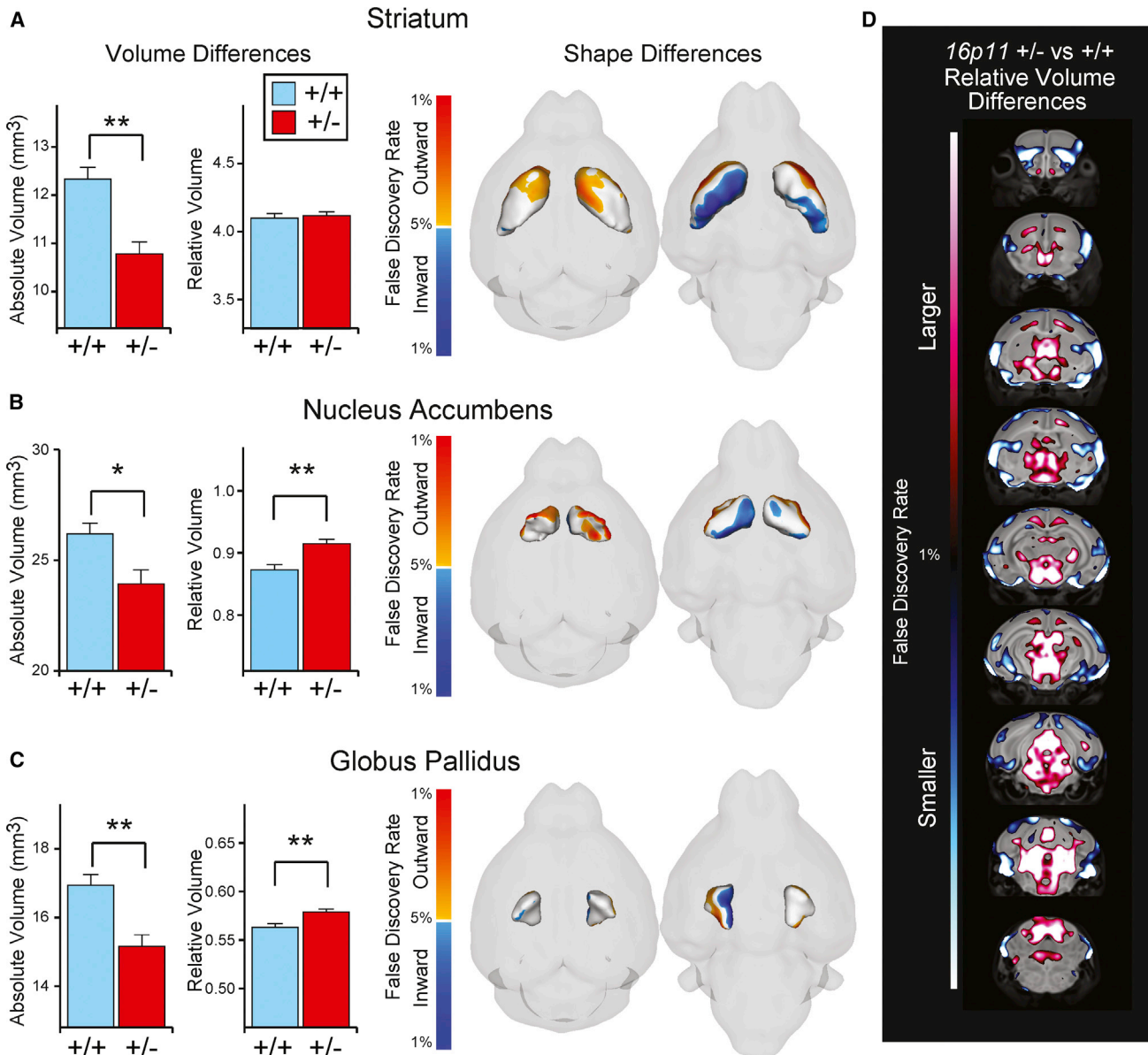


Figure 2. Anatomical Abnormalities in Juvenile $16p11^{+/-}$ Mice

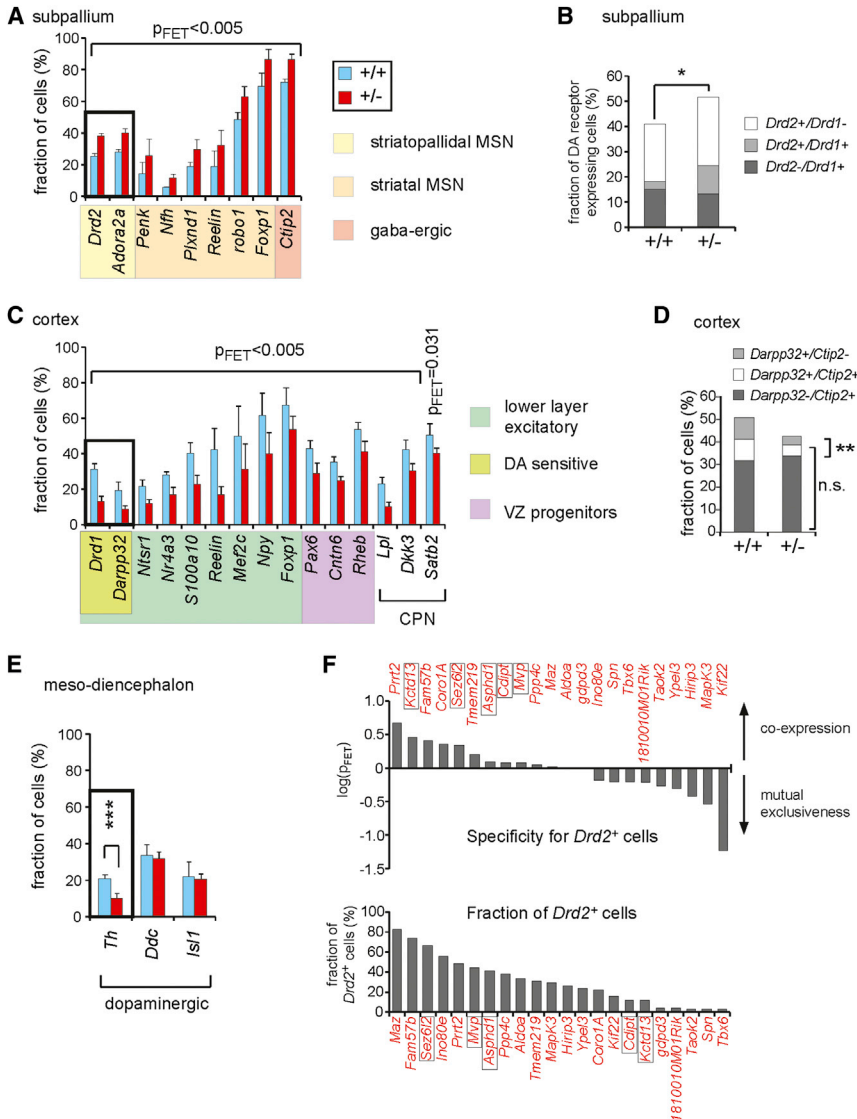
MRI analysis of mouse brains at P7 ($n = 26$ for each genotype).

(A–C) Volume and shape difference are displayed for the BG regions, namely, the striatum (A), GP (B), and NAc (C). Volumes in (A)–(C) are shown as both absolute (in mm^3) and relative volumes. Shape differences in (A)–(C) show 3D surface renderings of the given region of interest. Highlighted on that surface are significant shape differences ($q < 0.05$) between the $16p11^{+/-}$ mouse and control. Orange, outward movement; blue, inward movement.

(D) Coronal flythrough highlighting significant differences in the relative volume of the $16p11^{+/-}$ mouse and control (red: larger, blue: smaller); only highly significant areas are shown ($q < 0.01$). Error bars represent SEM. * $q < 0.05$, ** $q < 0.01$.

3E). However, when we quantified the cellular composition we found striking differences between $16p11^{+/-}$ and wild-type mice (Figures 4 and S3). There was a significant increase in the number of MSNs expressing *Drd2* in $16p11^{+/-}$ mice (+47.3%, $p = 0.003$; Figure 4A). This population of cells also expresses *Adora2a* (+43.0%, $p = 0.005$), as well as other markers of GABAergic and MSN identity, such as *Penk* (+83.4%, $p = 0.002$), *Nfth* (+111.7%, $p = 0.005$), *Plxnd1* (+58.4%, $p = 0.001$), *Reelin* (+71.1%, $p = 1 \times 10^{-4}$), *Robo1* (+29.5%, $p = 3 \times 10^{-4}$),

Foxp1 (+24.1%, $p = 3 \times 10^{-7}$), and *Ctip2* (+20.2%, $p = 3 \times 10^{-6}$). The number of cells coexpressing all of these genes was significantly elevated, providing evidence for a general increase in the number of *Drd2*⁺ MSNs and not just an increase in *Drd2* expression resulting in higher chance of detection. Furthermore, the increase in *Drd2*⁺ MSNs was not at the expense of the *Drd1*⁺ MSN population, because we found no significant change *Drd1*⁺ cell numbers in the $16p11^{+/-}$ subpallium ($p = 0.086$) but observed an overall increase in the total number of cells expressing either



Drd2 and/or *Drd1* ($p = 0.017$, Figure 4B), suggesting an increased MSN pool in the striatum. Interestingly, we also observed an increased number of cells that coexpress both *Drd1* and *Drd2* in *16p11*^{+/-} mice ($p = 4 \times 10^{-4}$). These cells were rarely observed in wild-type mice suggesting that the *16p11*^{+/-} mutation alters not only the number of *Drd2*⁺ MSNs, but also the process of MSN specification.

Although *Drd1*⁺ cell numbers were not reduced in the striatum, we observed a significant decrease in *Drd1*⁺ cells in the cortex

Figure 4. Altered DA Signaling in the Neonate 16p11^{+/-} Brain

(A) Numbers of subpallial cells expressing genes specific to GABAergic neurons, striatal MSNs, and striatopallidal MSNs suggest an increase in the number of indirect pathway MSNs and total MSNs in *16p11*^{+/-} mice.

(B) Striatal MSNs as defined by DA receptor gene expression only. Note that the increase in *Drd2*⁺ MSNs is not at the expense of *Drd1*⁺ cells, but is likely due to a total increase in the number of MSNs consistent with (A).

(C) Abnormalities in deeper layer cortical excitatory neurons and *Pax6*⁺ VZ progenitors as well as callosal projection neurons (CPN). Reduction of *Darpp32* and *Drd1* expression indicate a loss of dopamine-sensitive cells.

(D) Combined consideration of *Ctip2* and *Darpp32* expression suggests a lower number of dopamine-sensitive cells in the deeper cortical layers but no major reduction in deeper layer corticofugal cell types. n.s., not significant.

(E) Decreased expression of *Th* in ventral midbrain DA cells.

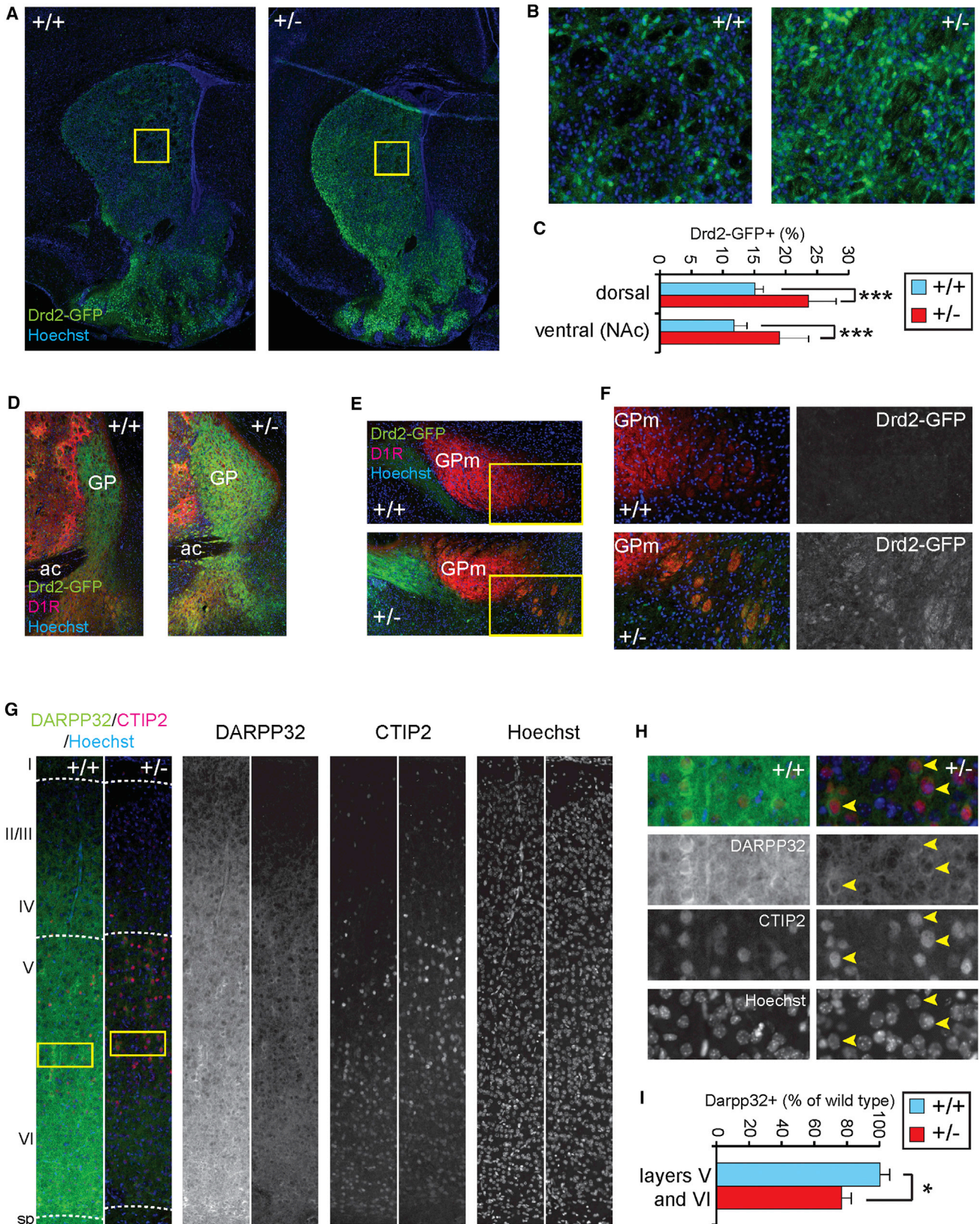
(F) Top: coexpression of the *16p11* genes in striatopallidal MSNs as defined by *Drd2* expression. Framed *16p11* genes have been reported in ASD individuals with a smaller deletion in the *16p11.2* locus. Bottom: fraction of *Drd2*⁺ cells expressing each of the *16p11* genes.

Error bars represent SEM. * $p < 0.05$, ** $p < 0.01$, and *** $p < 0.001$ where not otherwise indicated.

(-58.2%, $p = 1 \times 10^{-6}$; Figure 4C). This reduction was accompanied by reduction of another marker for DA-sensitive deeper layer excitatory neurons, *Darpp32* (-55.6%, $p = 9 \times 10^{-5}$), as well as a battery of other genes specific to deeper layer neurons, including *Ntsr1* (-44.1%, $p = 0.001$), *Nr4a3* (-39.4%, $p = 9 \times 10^{-4}$), *S100a10* (-44.1%, $p = 2 \times 10^{-6}$), *Reelin* (-60.0%, $p = 4 \times 10^{-12}$), *Mef2c* (-37.6%, $p = 1 \times 10^{-5}$), *Npy* (-35.5%, $p = 8 \times 10^{-8}$), and *Foxp1* (-20.4%, $p = 9 \times 10^{-4}$). Importantly, based on the expression of *Ctip2*, a marker specific for corticofugal projecting cell types such as corticospinal motor neurons, not all deeper layer neurons appeared equally affected. We found no major reduction in *Ctip2*⁺ cells, but fewer *Ctip2*⁺ cells coexpressing *Drd1* and *Darpp32* (Figure 4D), again pointing toward a reduction in DA sensitivity in these cells. Furthermore, we observed a downregulation of genes in the cluster specific

Figure 3. Single-Cell Gene Expression Profiling of Cell Types in the Neonate Brain

(A) Experimental workflow: brain dissection, single-cell sorting by FACS, reverse transcription (RT), and preamplification of cDNAs of interest. A total of 190 genes were profiled by multiplex qPCR using two 96.96 dynamic arrays per sample plate. ctx, cortex; hc, hippocampus; spa, subpallium; ms-dienc, mesodiencephalon. (B and C) Identification of cell-type-specific gene clusters for the subpallium (B) and cortex (C) by coexpression mapping ($n > 500$ cells). The dendrogram shows the proximity of genes based on their coexpression with all other genes. Listed genes are known to be expressed in a cell-type- and/or developmental-stage-specific manner and used accordingly for identification of cell-type-specific gene clusters. (D and E) Separate clustering for *16p11*^{+/-} and wild-type samples ($n \approx 250$ cells each) of subpallium (D) and cortex (E). Color code matches (C) and (D), respectively. LVW, lateral ventricular wall; LMS, lateral migratory stream; SVZ, subventricular zone; VZ, ventricular zone.



(legend on next page)

to ventricular zone (VZ) progenitors, particularly *Pax6* (−32.9%, $p = 2 \times 10^{-4}$), and three genes reported to be specific to callosal projection neurons (CPN), *Lpl* (−56.9%, $p = 7 \times 10^{-6}$), *Dkk3* (−28.2%, $p = 0.002$), and *Satb2* (−54.0%, $p = 0.031$) (Alcamo et al., 2008; Molyneaux et al., 2009) (Figure 4C). The latter result was corroborated by immunohistochemical staining in P7 mice showing reduced numbers of SATB2⁺ neurons (−18.4% $p = 0.0014$, Figures S4A and S4B) in *16p11*^{+/-} brains compared to wild-type. Furthermore, the results are consistent with data from diffusion tensor imaging indicating morphological abnormalities in the corpus callosum of *16p11*^{+/-} pups (Figures S4C and S4D).

sc-qPCR also revealed changes in the expression of specific genes in *16p11*^{+/-} mice independent of gene clusters. For example, tyrosine-hydroxylase (*Th*), which encodes a rate-limiting enzyme in the DA synthesis pathway, was decreased in mesodiencephalic DA cells (−52%, $p = 0.001$), although other genes expressed in this cell lineage, such as dopa-decarboxylase (*Ddc*) and *Isl1*, respectively, were unaffected (Figure 4E). Together, our results from multiplex sc-qPCR indicate a major imbalance in the DA signaling system of *16p11*^{+/-} mice.

Finally, we examined which of the *16p11* genes are expressed in the *Drd2*⁺ MSNs and therefore might be important for the defect observed in the mice (Figure 4F). We found that *Kctd13* ($p = 0.407$), *Prrt2* ($p = 0.227$), *Fam57b* ($p = 0.401$), *Sez6l2* ($p = 0.456$), and *Coro1a* ($p = 0.350$) are enriched in *Drd2*⁺ cells, whereas *Kif22* ($p = 0.058$), *Hirip3* ($p = 0.394$), *Mapk3* ($p = 0.293$), and *Ypel3* ($p = 0.516$) or *Tack2* ($p = 0.542$) show increased specificity for other cell types at this developmental stage. Interestingly, *Kctd13* and *Sez6l2* are located within a smaller *16p11.2* deletion of a patient diagnosed with ASD and *Kctd13* was identified as a gene that controls neuronal progenitor proliferation in zebrafish (Golzio et al., 2012).

Neuroanatomical Analysis of *Drd2*⁺ Cells

To independently determine whether the *16p11.2* deletion caused increased numbers of *Drd2*⁺ cells in the striatum, we crossed the *16p11*^{+/-} mice with *Drd2-EGFP* BAC transgenic (Gong et al., 2003) mice that express GFP under control of the *Drd2* gene-regulatory region, specifically in striatopallidal MSNs. We examined brains of *Drd2-EGFP*^{tg/+}; *16p11*^{+/-} mice at P7, when most structures of the brain have reached relatively definitive morphology and major migratory streams and projections have arrived at their target regions. We found a significant increase in the fraction of GFP⁺ cells in mutant

Drd2-EGFP^{tg/+}; *16p11*^{+/-} mice in both the ventral and dorsal striatum (+60.6%, $p = 1.7 \times 10^{-5}$ and +56.4%, $p = 2.3 \times 10^{-7}$ respectively) compared to controls (*Drd2-EGFP*^{tg/+}; *16p11*^{+/+}, Figures 5A–5C). In addition, we observed severe enlargement of the GP (Figure 5D), which receives input from *Drd2*⁺ MSNs, as well as ectopic GFP⁺ projections to GPm, which normally receives input from striatal *Drd1*⁺ cells (Figures 5E and 5F). This suggests that heterozygous deletion of the *16p11* genes results in aberrant expression of *Drd2* in cells projecting along the direct pathway to the GPm. Furthermore, antibody staining against DARPP32 to label DA-sensitive neurons in cortex of *16p11*^{+/-} mice revealed a significant loss of DARPP32 expression in deep layers (−23.6%, $p = 0.0149$, Figures 5G–5I), consistent with our sc-qPCR results. Finally, we tested whether above described cellular phenotypes could be validated in an independent, previously described *16p11.2* deletion mouse model (*16p11.2*^{df/+}) (Horev et al., 2011). *16p11.2*^{df/+} mice were bred with *Drd1a-TdTomato*^{tg/+} and subsequently with *Drd2-EGFP*^{tg/+} mice. Juvenile (P7) *Drd1a-TdTomato*^{tg/+}; *Drd2-EGFP*^{tg/+}; *16p11.2*^{df/+} animals displayed increased numbers of GFP⁺ MSNs and decreased numbers of TdTomato-expressing deep layer cortical neurons as compared to controls (*Drd1a-TdTomato*^{tg/+}; *Drd2-EGFP*^{tg/+}; *16p11.2*^{+/+}, Figures S5A–S5E). Taken together, these findings confirm our single-cell study and support the idea that the *16p11.2* deletion affects DA-sensitive neuronal circuits.

Electrophysiology of Striatal MSNs

We next examined whether changes in the DA-sensitive circuitry of the developing *16p11*^{+/-} brain affected the function of striatal MSNs by performing electrophysiological recordings from MSNs in the NAc while stimulating striatal afferents. AMPA receptor-mediated excitatory postsynaptic currents (AMPA EPSCs) revealed comparable I/V relationships in *16p11*^{+/-} and wild-type mice (Figure 6A) and thus no significant change in the AMPAR EPSC rectification index (defined as current amplitude at +40 mV over the current amplitude at −70 mV) (Figure 6B). This suggests that the stoichiometry of synaptic AMPARs in ventral striatal MSNs is unaffected in *16p11*^{+/-} mice and that the vast majority of these AMPARs contain the GluA2 subunit. However, a clear increase in the ratio of the AMPAR EPSC to NMDA receptor-mediated EPSC (AMPA/NMDAR ratio) was observed in *16p11*^{+/-} MSNs (Figure 6C), in addition to a significant decrease in the paired-pulse ratios (PPRs) across multiple interstimulus intervals (ISIs) (Figure 6D). Miniature AMPAR

Figure 5. Excess Numbers of Striatopallidal MSNs and Hypodopaminergia in Cortex of Juvenile *16p11*^{+/-} Mice

- (A) Coronal cryosections show the expression of a *Drd2-GFP* BAC transgene in the mouse striatum at P7.
 (B) Magnification of boxed regions of the dorsal striatum from (A).
 (C) Quantification of GFP⁺ cells ($n = 3$ animals per genotype).
 (D) The GP, the output structure of striatopallidal projecting (*Drd2*⁺) MSNs, is enlarged in *16p11*^{+/-} brains.
 (E) GPm, the striatonigral (*Drd1*⁺ MSNs) output structure contains *Drd2-GFP*⁺ fibers in *16p11*^{+/-} not found in wild-type.
 (F) Magnification of boxed regions in (E).
 (G) Somatosensory cortex in sagittal sections of P7 brains shows downregulation of DARPP32 expression. CTIP2 was used for visualization of layer V (large, bright CTIP2⁺ pyramidal neurons), and layer VI (smaller, less bright CTIP⁺ neurons). Blue: Hoechst nuclear stain.
 (H) Magnification of boxed area in (G). Although DARPP32 expression is much weaker in *16p11*^{+/-} cortex, some DARPP32⁺ cells can still be identified (yellow arrowheads).
 (I) Quantification of DARPP32⁺ cells in cortical layers V and VI (irrespective of expression level).
 Error bars represent SEM. * $p < 0.05$, ** $p < 0.01$, and *** $p < 0.001$.

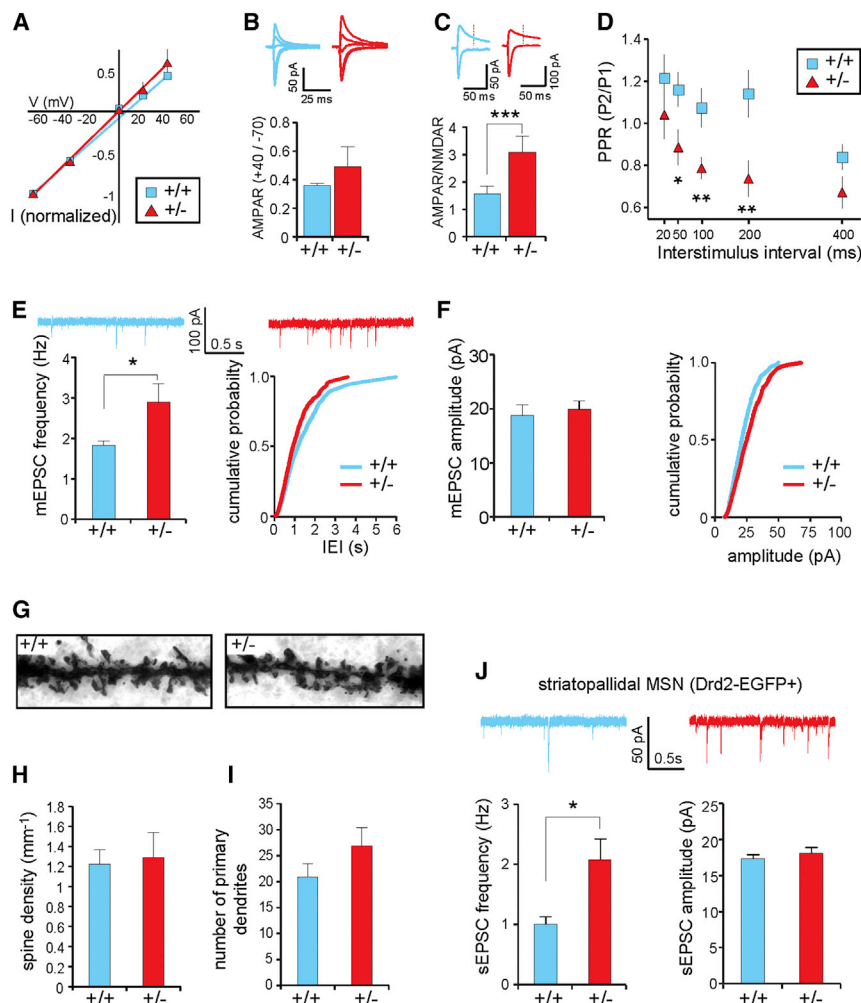


Figure 6. Deficits at Excitatory Synapses onto NAc MSNs in $16p11^{+/-}$ Mice

Electrophysiological recordings in NAc MSNs at 4–8 weeks.

(A and B) Comparable I/V relationships (A) AMPAR rectification index (B) in $16p11^{+/-}$ and wild-type mice ($n = 9$ cells for each genotype).

(C) Increased AMPAR/NMDAR ratio in $16p11^{+/-}$ mice.

(D) Decreased paired-pulse ratios (PPRs) across multiple interstimulus intervals (ISIs) in $16p11^{+/-}$ mice.

(E) Consistent with a higher presynaptic release probability, significant increase in mEPSC frequency in $16p11^{+/-}$ mice ($n = 12$ wild-type cells, $n = 14$ $16p11^{+/-}$ cells).

(F) Comparable mEPSC amplitude between genotypes.

(G–I) Morphological analysis (8 weeks of age) of MSN dendrites ($n = 10$ cells per genotype). (G) Representative Golgi-stained MSN dendrites covered with dendritic spines. (H and I) No change in spine density (H) or number of primary dendrites (I) was detected.

(J) Recording of synaptic events in *Drd2-EGFP*⁺ MSNs of the $16p11^{+/-}$ NAc (4–6 weeks) show a significant increase in sEPSC frequency, whereas the amplitude remained unchanged ($n = 9$ wild-type cells, $n = 10$ $16p11^{+/-}$ cells).

Error bars represent SEM. * $p < 0.05$, ** $p < 0.01$, and *** $p < 0.001$.

(Grueter et al., 2010; Kreitzer and Malenka, 2007). The decreased PPR and increased mEPSC frequency could thus be a result of oversampling indirect-pathway MSNs in $16p11^{+/-}$ mice, due to the increased number of D2R-expressing cells. To test this, we again used the

EPSC (mEPSC) recordings further showed an increase in the mean mEPSC frequency (wild-type: 1.82 ± 0.19 , $16p11^{+/-}$: 2.90 ± 0.45 , $p = 0.039$) (Figure 6E). The mean mEPSC amplitude was not significantly changed in $16p11^{+/-}$ MSNs (wild-type: 18.64 ± 2.14 , $16p11^{+/-}$: 19.76 ± 1.27 , $p = 0.540$) (Figure 6F). In summary, the decrease in PPRs and increase in mEPSC frequency in $16p11^{+/-}$ MSNs strongly suggest that the release probability of excitatory synapses on MSNs is increased. The increased AMPAR/NMDAR ratio suggests that excitatory synapses on $16p11^{+/-}$ MSNs also exhibit postsynaptic alterations. These may include increase in quantal size preferentially at synapses with mEPSCs below our detection threshold. Although these physiological measurements demonstrate that $16p11^{+/-}$ MSNs exhibit changes in excitatory synaptic function, they do not address the possibility of additional morphological changes in striatal MSNs. However, analysis of MSN primary dendrite number and spine density indicated no significant differences between wild-type and $16p11^{+/-}$ (Figures 6G–I).

Previous studies have suggested that release probability at excitatory synapses terminating on indirect-pathway MSNs is higher than at synapses terminating on direct-pathway MSNs

Drd2-EGFP BAC transgene to specifically target indirect-pathway MSNs by recording from *GFP*⁺ neurons in the NAc. We observed a significantly increased EPSC frequency (sEPSCs) recorded in *GFP*⁺ MSNs of mutants compared to wild-type (*Drd2-EGFP*^{tg/+}; $16p11.2^{+/-}$: 2.07 ± 0.35 ; *Drd2-EGFP*^{tg/+}; $16p11.2^{+/+}$: 1.0 ± 0.13 ; $p < 0.02$) (Figure 6J). These data argue against oversampling of *Drd2*⁺ neurons as an explanation for the observed electrophysiological phenotype in $16p11^{+/-}$ striatum and instead argue for a fundamental alteration in ventral striatal circuitry.

Behavioral Analysis

DA pathways in the BG are important for motor, emotional, and cognitive function. The changes in DA signaling and striatal circuitry observed in $16p11^{+/-}$ mice suggest possible mechanisms relevant for deficits observed in $16p11.2$ deletion syndrome. We therefore tested $16p11^{+/-}$ mice in a battery of behaviors to assay defects in locomotor activity, social interaction, working memory, and sensory processing. To control for variability across testing sites, these studies were conducted in parallel by the Stanford Behavioral and Functional

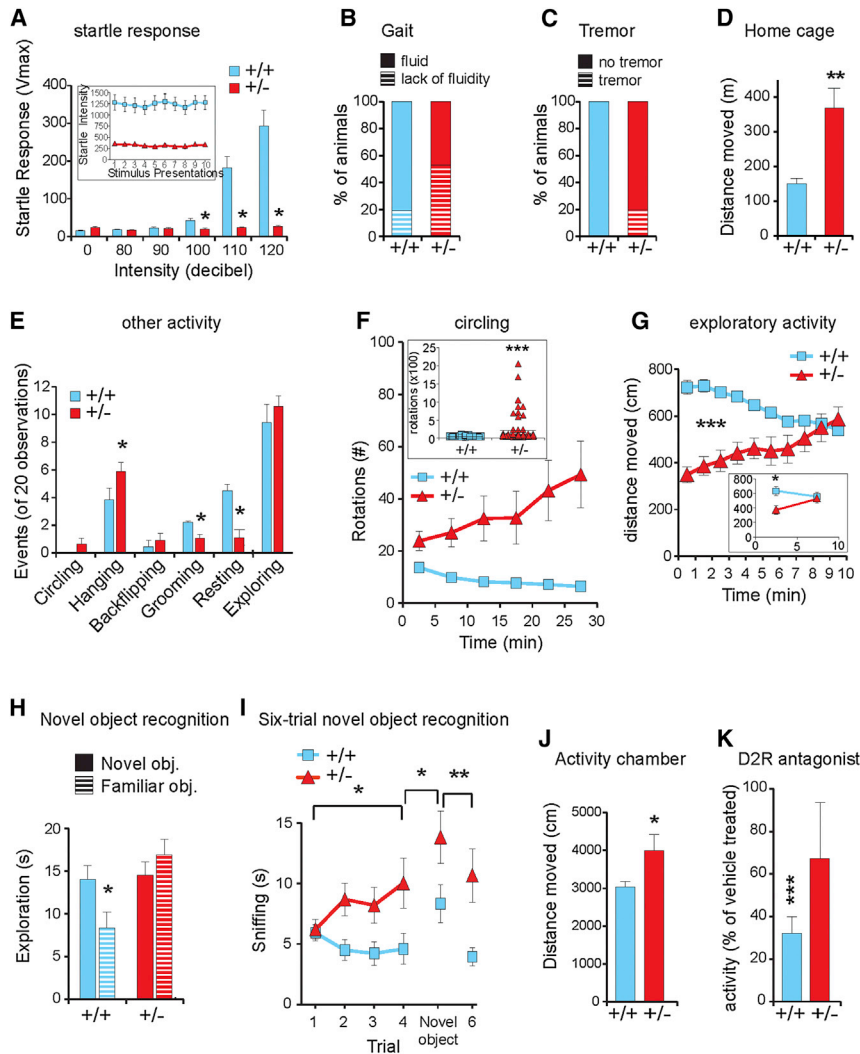


Figure 7. Behavioral Deficits of Adult $16p11^{+/-}$ Animals

(A) Adult $16p11^{+/-}$ mice (2–3 months) display a significantly reduced startle response at increasing decibels (NIMH: wild-type $n = 17$, $16p11^{+/-}$ $n = 15$) and repeated 20-stimulus presentations (inset, SBFNL).

(B and C) Movement control: $16p11^{+/-}$ mice show lack of gait fluidity (B) and frequent tremor (C).

(D) Hyperactivity of $16p11^{+/-}$ mice in a home-cage environment.

(E) In a novel empty-cage environment, $16p11^{+/-}$ mice exhibited significantly more hanging, less self-grooming, and less resting than wild-type littermates. A fraction of $16p11^{+/-}$ mice showed continuous circling.

(F) Follow-up quantification of circling behavior in a rotational assay in a cylindrical cage (inset, total number of rotations over the 30 min period).

(G) Adult $16p11^{+/-}$ mice exhibited initial hypoactivity and abnormal dishabituation to novel environment in the open field. Inset, similar behaviors of the $16p11^{+/-}$ mice in the open-field test independently reproduced at NIMH.

(H and I) Adult $16p11^{+/-}$ mice display altered performance in a novel object recognition test (H) and a six-trial novel object recognition assay (I) compared to wild-type littermates. $16p11^{+/-}$ mice did not show a significant preference for the novel object, compared to wild-type mice (H). This effect was due to a lack of habituation to the familiar object in the $16p11^{+/-}$ mice. This was further corroborated in a six-trial novel object recognition test, where the $16p11^{+/-}$ mice spent longer time in trials 2–4 and 6 sniffing the first object that had been presented as a novel object in trial 1 and also longer time sniffing the second novel object in trial 5 than the control mice (I).

(J) Adult $16p11^{+/-}$ mice showed hyperactivity in the activity chamber during a 10 min period.

(K) Acute administration of risperidone had no significant effect on the activity level of $16p11^{+/-}$ mice in the activity chamber, whereas wild-type littermates exhibited a dramatic decrease in activity level after risperidone administration.

For all panels, mean \pm SEM is presented for each data point; * $p < 0.05$, ** $p < 0.01$, and *** $p < 0.001$. (A), (E), (G) inset, and (H): NIMH; (A) inset, (B)–(D), (F), (G), and (I)–(K): SBFNL.

Neuroscience Laboratory (SBFNL) and by the Laboratory of Behavioral Neuroscience at the National Institute of Mental Health (NIMH). Tests were performed on increasing C57BL/6N background after hybrid founder mice had been backcrossed into C57BL/6N for at least five to seven times.

Eight- to 12-week-old $16p11^{+/-}$ mice did not show gross defects in a battery of tests for general health and neurological reflexes (Tables S3 and S4; Figure S6A). The mice also had normal olfactory abilities, as assessed in the olfactory habituation/dishabituation test (Figure S6B), and normal vision, as assessed by the forepaw reaching test (Table S3). However, $16p11^{+/-}$ mice lacked a startle response even to sounds at 120 dB (NIMH: at 100 dB, $F_{1,30} = 8.04$, $p < 0.01$; at 110 dB, $F_{1,30} = 29.1$, $p < 0.001$; at 120 dB, $F_{1,30} = 28.2$, $p < 0.001$, Figure 7A). This change was likely due to a defect in auditory perception or processing because the mice had normal startle responses to air puffs but had defects in evoked electrical responses (not shown).

Motor Behavior

Although the analysis of gait and locomotor activity in adult $16p11^{+/-}$ mice showed normal performance in a rotarod test (Figures S6C and S6D), a significant fraction of mice displayed tremor ($16p11^{+/-}$: 19.4%, $p < 0.001$) and a decrease in fluid gait (wild-type: 19.4%, $16p11^{+/-}$: 52.8, $p < 0.001$, Figures 7B and 7C). These findings are consistent with tremor and severe motor coordination defects observed in 10-day-old pups (Movie S1) and suggest an underlying developmental defect rather than a neurodegenerative process.

We next investigated activity patterns in a home-cage environment in the dark using the PhenoTyper system for 4 hr. The $16p11^{+/-}$ mice moved approximately 2.5 times the distance of wild-type littermates (Figure 7D; effect of genotype: $F_{1,11} = 26.57$, $p = 0.003$; effect of time: $F_{3,33} = 12.78$, $p < 0.0001$; effect of genotype \times time interaction $F_{3,33} = 0.659$, NS; overall distance moved: $t_{11} = 5.15$, $p = 0.003$). $16p11^{+/-}$ mice also exhibited more bouts of hanging ($U = 380.5$, $p < 0.05$), less self-grooming

($U = 385.0$, $p < 0.02$), and less resting ($U = 369.5$, $p < 0.05$) compared to wild-type in the home cage (Figures 7E and S6E). In addition, we observed a significant increase in circling behavior in a fraction (18.75%) of $16p11^{+/-}$ mice (Figure 7F, $t_{131} = 3.404$, $p < 0.0001$). These behaviors are indications of significant hyperactivity in $16p11^{+/-}$ mice in an otherwise dark, low-stress, and familiar environment.

In contrast, when observed in an open-field test, under bright light in a novel environment, the $16p11^{+/-}$ mice showed initial hypoactivity that gradually disappeared over the course of the first 10 min as well as a lack of habituation to the novel environment (Figure 7G, effect of genotype: $F_{1,86} = 17.72$, $p < 0.0001$). Based on analysis of the time spent in the center versus in the periphery of the chamber, we found no evidence that this initial hypoactivity reflected increased anxiety (Figure S6F). The initial hypoactivity of $16p11^{+/-}$ mice in the open-field test might therefore reflect deficits related to motor initiation rather than anxiety.

Social Behavior

In humans, activity in the striatal circuits has been correlated with social deficits relevant to autism (Cascio et al., 2012; Insel, 2003). Normal sociability was detected in multiple cohorts of adult $16p11^{+/-}$ mice in a three-chamber social interaction test (Figure S7). Both sexes exhibited significant sociability as well as preference for social novelty spending significantly more time in a chamber containing a mouse than in one containing an object (sociability test) and more time in a chamber containing an unfamiliar mouse than one containing a familiar mouse (social novelty test). Quantification of sniffing time in these two tests corroborated chamber time data. Similar results were obtained on reciprocal social interactions with two cohorts of juvenile mice (stage P21–P25, Figure S6J). Overall, these results indicate largely normal social interactions in $16p11^{+/-}$ mice.

Novelty-Seeking Behavior

Autism is also associated with a preference for sameness and an aversion to novelty. Wild-type mice seek novel objects and spend more time with novel objects than familiar ones. In addition, they gradually lose interest in familiar objects over time (habituation). In a conventional novel object recognition test to determine if mice learn and remember familiar versus unfamiliar objects (Figure 7H), we exposed control and $16p11^{+/-}$ mice first to two identical objects and then 1 hr later to one of the now-familiar identical objects and one new object and quantified the time that each genotype spent sniffing each object. Wild-type mice spent significantly more time sniffing the novel object than the familiar object ($F_{1,23} = 16.16$, $p < 0.001$), indicating normal learning and memory, whereas $16p11^{+/-}$ mice did not display any preference for the novel object over the familiar object ($F_{1,25} = 1.07$, NS), indicating a cognitive deficit (Figure 7H). Two standard cognitive tasks could not be conducted, the Morris water-maze task because the $16p11^{+/-}$ mice frequently sank rather than swimming when placed in the pool, and fear conditioning because of the hearing deficit (Figures S6G and 7A, respectively). In other tests performed to evaluate memory, the $16p11^{+/-}$ mice were indistinguishable from control mice in their performance (Y maze and a modified Barnes Maze, Figures S6H and S6I). We then tested whether $16p11^{+/-}$ mice become

desensitized to novel objects by presenting control and $16p11^{+/-}$ mice with the same object four times with 10 min inter-trial interval (ITI), followed by presentation of a novel object, and then reintroduction of the familiar object (Figure 7I). Although control mice showed normal habituation to the novel object, $16p11^{+/-}$ mice showed increased interest for the familiar object that did not decline over the course of presentations (effect of genotype $F_{1,68} = 5.99$, $p = 0.017$; effect of genotype \times trial interaction $F_{3,204} = 3.92$, $p < 0.01$). This result suggests that $16p11^{+/-}$ mice lack the habituation normally observed in response to novel objects.

Effects of Risperidone on Activity Levels

The importance of BG function in motor control suggests a correlation of the increased numbers of $Drd2^+$ cells in the striatum with the hyperactivity of $16p11^{+/-}$ mice. We therefore treated $16p11^{+/-}$ mice with risperidone, a D2R antagonist used clinically in patients with ASD. Risperidone has multiple effects in mice but primarily acts as a sedative. We introduced $16p11^{+/-}$ and control mice into an activity chamber in a standard, low-stress assay for base-line activity similar to home cage performed in the dark. The $16p11^{+/-}$ mice moved significantly more than control mice over the course of 10 min (Figure 7J). We then injected the mice with either saline vehicle or 0.2 mg/kg of risperidone and again observed their activity over the course of 10 min. Injection of risperidone significantly decreased the activity levels of wild-type mice (Figure 7K, $t_{40} = 7.41$, $p < 0.0001$) but had no significant effect on those of $16p11^{+/-}$ mice ($t_{39} = 1.44$, NS). Consistent with this, acute administration of risperidone had no overt effect on circling behavior in a subgroup of the $16p11^{+/-}$ mice (not shown). This suggests that $16p11^{+/-}$ mice are less susceptible to sedation by this D2R antagonist.

DISCUSSION

We have generated a mouse model for the 16p11.2 microdeletion syndrome and identified a set of anatomical, behavioral, and electrophysiological phenotypes that provide insights into the developmental consequences of this mutation. In agreement with a previous paper describing a different mouse with the same deletion, we found that the $16p11^{+/-}$ mice are born at Mendelian ratios, have impaired early-postnatal survival, are smaller than wild-type mice and are hyperactive. However, by using a comprehensive set of tools at ASD-relevant developmental stages we uncovered cellular and behavioral defects that significantly expand our knowledge of the phenotypic consequences of this deletion.

Anatomically we found abnormalities in the BG circuitry, namely, striatum and GP, as well as direct BG input (cortex) and output (thalamus and superior colliculus) structures. Using in vivo high-throughput single-cell gene expression profiling, we identified developmental changes in the BG- and DA-regulated circuitry of $16p11^{+/-}$ mice, including increased numbers of $Drd2^+$ MSNs in the striatum and downregulation of DA signaling components ($Drd1$ and $Darpp32$) in deeper cortical layers. Furthermore, expression of Th in cells of the mesodiencephalon was decreased. These abnormalities were accompanied by both pre- and postsynaptic defects at NAc MSNs as

assessed by electrophysiology. Overall, these changes likely contribute to severe motor deficits observed in juvenile and adult $16p11^{+/-}$ mice, including hyperactivity in a home-cage environment, tremor, lack of gait fluidity, and circling. Furthermore, a behavioral correlate of the increased numbers of striatopallidal MSNs is provided by the significantly reduced sensitivity of $16p11^{+/-}$ mice to the D2R antagonist risperidone. This differential effect of risperidone suggests involvement of indirect pathway deficits in the abnormal activity pattern of $16p11^{+/-}$ mice and thus provides evidence for another link between cellular and behavioral deficits in these mice. The $16p11^{+/-}$ mice also showed a lack of habituation to familiarity in experiments testing novelty recognition, in the absence of overt memory defects. Taken together, these findings strongly indicate that the 16p11.2 deletion alters the gross developmental trajectory of the brain, including anatomy, connectivity, and information processing by the BG as well as circuit modulation by DA. Nevertheless, despite compelling evidence for the involvement of disrupted BG function in the phenotypes of $16p11^{+/-}$ mice, other brain regions, including—but not limited to—input and output structures of the BG, may also contribute. Our study provides evidence that BG function is altered by the 16p11.2 deletion and may provide important clues about the underlying basis of ASD and other psychiatric disorders.

Comparison of 16p11.2 Deletion in Mice and Humans

There are several similarities and notable differences between our mouse model and patients with 16p11.2 deletions. MRI data suggest a relative increase in size of various brain regions, including nuclei of the BG and mesodiencephalon. This could be seen as a parallel to the frequently described macrocephaly in human 16p11.2 deletion patients and other types of ASD (Courchesne et al., 2007). There is also an apparent decrease in the size of the corpus callosum, which has been repeatedly observed in ASD and ADHD (Giedd et al., 1994; Gilliam et al., 2011), as well as mouse models for ASD (Ellegood et al., 2013; Wahlsten et al., 2003). The $16p11^{+/-}$ mice show hyperactivity, a potential correlate for ADHD observed in 16p11.2 patients (Shinawi et al., 2010). The mice also show defects in smooth motor movements that may be analogous to the highly prevalent motor delay described for 16p11.2 patients. Finally, defects in habituation to familiar objects are reminiscent of behavioral inflexibility reported in ASD. Together, these phenotypes suggest that the mouse model may provide some insights into the underlying circuits that lead to developmental defects in individuals with 16p11.2 deletions.

There are also a number of differences between the $16p11^{+/-}$ mouse and individuals with the 16p11.2 deletion. Patients have a tendency to be obese, whereas the $16p11^{+/-}$ mice are smaller and leaner than wild-type. Our early observations suggest reduced weight loss and improved growth performance of $16p11^{+/-}$ pups when littermate competition is decreased, making it unlikely that the abnormal weight of $16p11^{+/-}$ mice is related to mechanisms acting in humans, in which social and cultural factors eliminate a similar early postnatal selection pressure. Nevertheless, we cannot exclude the possibility that nutritional status of the pups could have affected postnatal brain development that may, in turn, have contributed to our observed

behavioral phenotypes. In conclusion, our mouse model for the 16p11.2 deletion exhibits many phenotypes suggestive of abnormal function in the BG- and DA-regulated circuits, with behavioral and anatomical parallels in human patients. Interpretation of the human deficits in light of abnormal BG function may be important for understanding the underlying molecular mechanisms and developing therapeutic approaches targeting cellular defects in 16p11.2 deletion patients.

EXPERIMENTAL PROCEDURES

A detailed description of all methods is provided in the [Supplemental Experimental Procedures](#) available online. All animal experiments were in accordance with the National Institutes of Health and Stanford guidelines for care and use of laboratory animals and approved by the National Institute of Mental Health Animal Care and Use Committee.

ESC Targeting

Sequential mouse ESC targeting was done according to standard protocols including LoxP sites (chr7:133842117 and chr7:134285222) and a fluorescent mCherry reporter transgene (Figures 1A–1D and S1A–S1K). Sequential targeting of DNA constructs resulted in both *cis* and *trans* arrangements of the LoxP sites in different mESC clones, as verified by PCR analysis of *Cre*-transfected ESC clones (Figures S1L and S1M). Germline transmission was successful only for the *cis* arrangement.

MRI Study

Diffusion tensor images of 52 brains ($16p11^{+/-}$ and 26 wild-type) were acquired on a 7 Tesla MRI scanner (Varian) using a custom built three coil solenoid array to acquire images from three brains in parallel (Nieman et al., 2007). Image averaging and registration, was used to provide measures of local differences in anatomy between mice. Multiple comparisons were controlled for by using the false discovery rate (FDR) (Genovese et al., 2002).

96.96 Dynamic Arrays, Data analysis, and Coexpression Mapping

sc-qPCR experiments and FACS sorting by the Stanford Shared FACS Facility were performed as previously described (Pasca et al., 2011; Yoo et al., 2011). A major challenge of single-cell gene expression analysis is the fluctuation of mRNA pools caused by transcriptional kinetics of individual alleles (Suter et al., 2011). A thorough assessment of the basic properties of the sc-qPCR data, which addressed (1) variability of gene expression level between single cells, (2) housekeeping genes and their value for normalization, (3) reflection of gene expression changes in the data, and (4) false-positives/negatives (Figures S2C–S2H; Supplemental Experimental Procedures), is provided in the [Supplemental Experimental Procedures](#). Across-chip normalization was done on the mean expression of the ubiquitous *Rps18* and *Gapdh* genes.

It remains unclear, given the biological difficulties we addressed earlier, what the value of the expression level of a cell-type-specific gene within a single cell is for classifying cell types. We therefore restricted our analysis to coexpression of genes. Data were clustered using the R-based heatmap tool (heatmap.2, R package: gplots) provided by Los Alamos National Laboratory (<http://www.hiv.lanl.gov>) and the manhattan distance between coexpression profiles of genes combined with Ward's clustering method (Ward, 1963). Gene clusters were associated with known cell types reported in the literature and publicly available gene expression repositories (including Allen Brain Atlas for developing mouse brain, at e18 and P4). An example for coexpression mapping is provided in [Supplemental Experimental Procedures](#).

Electrophysiology

Parasagittal slices (250 μ m) containing the NAc core were prepared from wild-type and $16p11^{+/-}$ mice on a C57BL/6N background (age P28–56), as described previously (Dölen et al., 2013).

Behavioral Assays at SBFNL

Age-matched *16p11^{+/-}* and wild-type mice were maintained on a C57BL/6N background, after backcrossing with C57BL/6N wild-type mice for five to seven generations. Four cohorts of male and female mice (aged 2–9 months) were blindly tested in behavioral paradigms. SHIRPA, home-cage behavioral monitoring, activity chamber, open field, grip strength, rotarod, startle response, Y maze spontaneous alternation task, modified Barnes maze, novel object recognition, three-chamber sociability and social novelty tasks, and associated statistical analyses were performed according to previously established protocols at SBFNL (Bader et al., 2011; Coutellier et al., 2012; Faizi et al., 2011, 2012; Ishizaki et al., 2010). For risperidone treatment, mice of both genotypes and genders were semirandomly divided into vehicle or risperidone treatment groups based on their activity levels in an activity chamber. One hour after acute, intraperitoneal risperidone administration (conc.: 0.2 mg/kg, vol.: 10 ml/kg) locomotor activity levels were measured for 10 min in the activity chamber.

Behavioral Assays at the NIMH

Twelve *16p11^{+/+}* females and six *16p11^{+/-}* males were transferred from Stanford University to the National Institute of Mental Health in Bethesda, MD, and bred as described in Supplemental Experimental Procedures to generate two cohorts for behavioral testing. Pup body weight, juvenile reciprocal social interactions, three-chambered social approach, general health and neurological reflexes, open-field activity, novel empty cage, acoustic startle response, olfactory habituation/dishabituation, and novel object recognition are fully described in the Supplemental Experimental Procedures and previous publications (Briellmaier et al., 2012; Chadman et al., 2008; Ey et al., 2012; Silverman et al., 2011; Yang et al., 2011, 2012; Yang and Crawley, 2009).

SUPPLEMENTAL INFORMATION

Supplemental Information includes Supplemental Experimental Procedures, seven figures, four tables, and one movie and can be found with this article online at <http://dx.doi.org/10.1016/j.celrep.2014.03.036>.

AUTHOR CONTRIBUTIONS

T.P. made the mice. M.Y., R.M., P.L.B., D.K., D.L., N.L.S., Z.Z., and M.A.M. performed and analyzed behavioral experiments; T.P. and G.P. performed sc-qPCR experiments and data analysis; J.E. and J.P.L. performed MRI experiments; T.P., G.P., E.F., K.C., and P.R. performed IHC stainings; G.D., B.A.G., and C.G. performed electrophysiological characterization; and R.E.D., J.N.C., M.S., R.C.M., T.P., M.Y., R.M., G.P., J.E., G.D., P.L.B., and J.P.L. planned the experiments and wrote the paper.

ACKNOWLEDGMENTS

We would like to thank Ulrich Elling and Josef Penninger (IMBA Vienna, Austria) for help and advice on mouse ESC targeting, Marty Bigos of the Stanford shared FACS facility for assistance with clone sorting, Renee Reijo-Pera for generously providing the Biomark Instruments, Kristin L. Sainani for advice in statistical analysis of mouse behavioral data, and Yishan Sun for validating and providing primer pairs for the single-cell gene expression analysis. This research was funded by the Simons foundation SFARI grant no. 204340 (R.E.D. and J.N.C.), Nina Jauw (R.E.D.), the Swiss National Science Foundation (nos. PBSKP3-123434 and PA00P3_134196, T.P.), the NIMH Intramural Research Program and the University of California Davis MIND Institute (M.Y., D.K., D.L., and J.N.C.), an F31 NRSA from the NIMH (no. MH090648-02, G.P.), a K99 from the NIH/NIMH (no. MH091160, R.M.), and the Institute of Neurological Disorders and Stroke P30 center core grant no. NS069375-01A1 (M.S.).

Received: May 6, 2013
Revised: February 6, 2014
Accepted: March 7, 2014
Published: May 1, 2014

REFERENCES

- Abrahams, B.S., and Geschwind, D.H. (2008). Advances in autism genetics: on the threshold of a new neurobiology. *Nat. Rev. Genet.* 9, 341–355.
- Alcamo, E.A., Chirivella, L., Dautzenberg, M., Dobрева, G., Fariñas, I., Groschedl, R., and McConnell, S.K. (2008). *Satb2* regulates callosal projection neuron identity in the developing cerebral cortex. *Neuron* 57, 364–377.
- Arlotta, P., Molyneaux, B.J., Chen, J., Inoue, J., Kominami, R., and Macklis, J.D. (2005). Neuronal subtype-specific genes that control corticospinal motor neuron development in vivo. *Neuron* 45, 207–221.
- Arlotta, P., Molyneaux, B.J., Jabaudon, D., Yoshida, Y., and Macklis, J.D. (2008). *Ctip2* controls the differentiation of medium spiny neurons and the establishment of the cellular architecture of the striatum. *J. Neurosci.* 28, 622–632.
- Bader, P.L., Faizi, M., Kim, L.H., Owen, S.F., Tadross, M.R., Alfa, R.W., Bett, G.C., Tsien, R.W., Rasmussen, R.L., and Shamloo, M. (2011). Mouse model of Timothy syndrome recapitulates triad of autistic traits. *Proc. Natl. Acad. Sci. USA* 108, 15432–15437.
- Baron-Cohen, S., Scott, F.J., Allison, C., Williams, J., Bolton, P., Matthews, F.E., and Brayne, C. (2009). Prevalence of autism-spectrum conditions: UK school-based population study. *Br. J. Psychiatry* 194, 500–509.
- Bengtsson, M., Ståhlberg, A., Rorsman, P., and Kubista, M. (2005). Gene expression profiling in single cells from the pancreatic islets of Langerhans reveals lognormal distribution of mRNA levels. *Genome Res.* 15, 1388–1392.
- Bijlsma, E.K., Gijsbers, A.C., Schuurs-Hoeijmakers, J.H., van Haeringen, A., Fransen van de Putte, D.E., Anderlid, B.M., Lundin, J., Lapunzina, P., Pérez Jurado, L.A., Delle Chiaie, B., et al. (2009). Extending the phenotype of recurrent rearrangements of 16p11.2: deletions in mentally retarded patients without autism and in normal individuals. *Eur. J. Med. Genet.* 52, 77–87.
- Briellmaier, J., Matteson, P.G., Silverman, J.L., Senerth, J.M., Kelly, S., Genestine, M., Millonig, J.H., DiCicco-Bloom, E., and Crawley, J.N. (2012). Autism-relevant social abnormalities and cognitive deficits in engrailed-2 knockout mice. *PLoS ONE* 7, e40914.
- Cascio, C.J., Foss-Feig, J.H., Heacock, J.L., Newsom, C.R., Cowan, R.L., Benningfield, M.M., Rogers, B.P., and Cao, A. (2012). Response of neural reward regions to food cues in autism spectrum disorders. *J. Neurodev. Disord.* 4, 9.
- Chadman, K.K., Gong, S., Scattoni, M.L., Boltuck, S.E., Gandhi, S.U., Heintz, N., and Crawley, J.N. (2008). Minimal aberrant behavioral phenotypes of neuroigin-3 R451C knockin mice. *Autism Res.* 1, 147–158.
- Chen, B., Wang, S.S., Hattox, A.M., Rayburn, H., Nelson, S.B., and McConnell, S.K. (2008). The *Fezf2-Ctip2* genetic pathway regulates the fate choice of subcortical projection neurons in the developing cerebral cortex. *Proc. Natl. Acad. Sci. USA* 105, 11382–11387.
- Courchesne, E., Pierce, K., Schumann, C.M., Redcay, E., Buckwalter, J.A., Kennedy, D.P., and Morgan, J. (2007). Mapping early brain development in autism. *Neuron* 56, 399–413.
- Coutellier, L., Beraki, S., Ardestani, P.M., Saw, N.L., and Shamloo, M. (2012). *Npas4*: a neuronal transcription factor with a key role in social and cognitive functions relevant to developmental disorders. *PLoS ONE* 7, e46604.
- de Anda, F.C., Rosario, A.L., Durak, O., Tran, T., Gräff, J., Meletis, K., Rei, D., Soda, T., Madabhushi, R., Ginty, D.D., et al. (2012). Autism spectrum disorder susceptibility gene *TAOK2* affects basal dendrite formation in the neocortex. *Nat. Neurosci.* 15, 1022–1031.
- DeLong, M., and Wichmann, T. (2009). Update on models of basal ganglia function and dysfunction. *Parkinsonism Relat. Disord.* 15 (Suppl 3), S237–S240.
- Ding, J.B., Oh, W.J., Sabatini, B.L., and Gu, C. (2012). Semaphorin 3E-Plexin-D1 signaling controls pathway-specific synapse formation in the striatum. *Nat. Neurosci.* 15, 215–223.
- Dölen, G., Darvishzadeh, A., Huang, K.W., and Malenka, R.C. (2013). Social reward requires coordinated activity of nucleus accumbens oxytocin and serotonin. *Nature* 501, 179–184.

- Ellegood, J., Babineau, B.A., Henkelman, R.M., Lerch, J.P., and Crawley, J.N. (2013). Neuroanatomical analysis of the BTBR mouse model of autism using magnetic resonance imaging and diffusion tensor imaging. *Neuroimage* 70, 288–300.
- Ey, E., Yang, M., Katz, A.M., Woldeyohannes, L., Silverman, J.L., Leblond, C.S., Faure, P., Torquet, N., Le Sourd, A.M., Bourgeron, T., et al. (2012). Absence of deficits in social behaviors and ultrasonic vocalizations in later generations of mice lacking neuroligin4. *Genes Brain Behav.* 11, 928–941.
- Faizi, M., Bader, P.L., Tun, C., Encarnacion, A., Kleschevnikov, A., Belichenko, P., Saw, N., Priestley, M., Tsien, R.W., Mobley, W.C., and Shamloo, M. (2011). Comprehensive behavioral phenotyping of Ts65Dn mouse model of Down syndrome: activation of β 1-adrenergic receptor by xamoterol as a potential cognitive enhancer. *Neurobiol. Dis.* 43, 397–413.
- Faizi, M., Bader, P.L., Saw, N., Nguyen, T.V., Beraki, S., Wyss-Coray, T., Longo, F.M., and Shamloo, M. (2012). Thy1-hAPP(Lond/Swe+) mouse model of Alzheimer's disease displays broad behavioral deficits in sensorimotor, cognitive and social function. *Brain Behav.* 2, 142–154.
- Fernandez, B.A., Roberts, W., Chung, B., Weksberg, R., Meyn, S., Szatmari, P., Joseph-George, A.M., Mackay, S., Whitten, K., Noble, B., et al. (2010). Phenotypic spectrum associated with de novo and inherited deletions and duplications at 16p11.2 in individuals ascertained for diagnosis of autism spectrum disorder. *J. Med. Genet.* 47, 195–203.
- Fombonne, E. (2003). The prevalence of autism. *JAMA* 289, 87–89.
- Genovese, C.R., Lazar, N.A., and Nichols, T. (2002). Thresholding of statistical maps in functional neuroimaging using the false discovery rate. *Neuroimage* 15, 870–878.
- Geschwind, D.H., and Levitt, P. (2007). Autism spectrum disorders: developmental disconnection syndromes. *Curr. Opin. Neurobiol.* 17, 103–111.
- Giedd, J.N., Castellanos, F.X., Casey, B.J., Kozuch, P., King, A.C., Hamburger, S.D., and Rapoport, J.L. (1994). Quantitative morphology of the corpus callosum in attention deficit hyperactivity disorder. *Am. J. Psychiatry* 151, 665–669.
- Gilliam, M., Stockman, M., Malek, M., Sharp, W., Greenstein, D., Lalonde, F., Clasen, L., Giedd, J., Rapoport, J., and Shaw, P. (2011). Developmental trajectories of the corpus callosum in attention-deficit/hyperactivity disorder. *Biol. Psychiatry* 69, 839–846.
- Golzio, C., Willer, J., Talkowski, M.E., Oh, E.C., Taniguchi, Y., Jacquemont, S., Reymond, A., Sun, M., Sawa, A., Gusella, J.F., et al. (2012). KCTD13 is a major driver of mirrored neuroanatomical phenotypes of the 16p11.2 copy number variant. *Nature* 485, 363–367.
- Gong, S., Zheng, C., Doughty, M.L., Losos, K., Didkovsky, N., Schambra, U.B., Nowak, N.J., Joyner, A., Leblanc, G., Hatten, M.E., and Heintz, N. (2003). A gene expression atlas of the central nervous system based on bacterial artificial chromosomes. *Nature* 425, 917–925.
- Grueter, B.A., Bransjo, G., and Malenka, R.C. (2010). Postsynaptic TRPV1 triggers cell type-specific long-term depression in the nucleus accumbens. *Nat. Neurosci.* 13, 1519–1525.
- Horev, G., Ellegood, J., Lerch, J.P., Son, Y.E., Muthuswamy, L., Vogel, H., Krieger, A.M., Buja, A., Henkelman, R.M., Wigler, M., and Mills, A.A. (2011). Dosage-dependent phenotypes in models of 16p11.2 lesions found in autism. *Proc. Natl. Acad. Sci. USA* 108, 17076–17081.
- Insel, T.R. (2003). Is social attachment an addictive disorder? *Physiol. Behav.* 79, 351–357.
- Ishizaki, T., Erickson, A., Kuric, E., Shamloo, M., Hara-Nishimura, I., Inácio, A.R., Wieloch, T., and Ruscher, K. (2010). The asparaginyl endopeptidase legumain after experimental stroke. *J. Cereb. Blood Flow Metab.* 30, 1756–1766.
- Kravitz, A.V., Tye, L.D., and Kreitzer, A.C. (2012). Distinct roles for direct and indirect pathway striatal neurons in reinforcement. *Nat. Neurosci.* 15, 816–818.
- Kreitzer, A.C., and Malenka, R.C. (2007). Endocannabinoid-mediated rescue of striatal LTD and motor deficits in Parkinson's disease models. *Nature* 445, 643–647.
- Lai, T., Jabaudon, D., Molyneaux, B.J., Azim, E., Arlotta, P., Menezes, J.R., and Macklis, J.D. (2008). SOX5 controls the sequential generation of distinct corticofugal neuron subtypes. *Neuron* 57, 232–247.
- Marin, O., Anderson, S.A., and Rubenstein, J.L. (2000). Origin and molecular specification of striatal interneurons. *J. Neurosci.* 20, 6063–6076.
- McCarthy, S.E., Makarov, V., Kirov, G., Addington, A.M., McClellan, J., Yoon, S., Perkins, D.O., Dickel, D.E., Kusenda, M., Krastoshevsky, O., et al.; Wellcome Trust Case Control Consortium (2009). Microduplications of 16p11.2 are associated with schizophrenia. *Nat. Genet.* 41, 1223–1227.
- Molnár, Z., and Cheung, A.F. (2006). Towards the classification of subpopulations of layer V pyramidal projection neurons. *Neurosci. Res.* 55, 105–115.
- Molyneaux, B.J., Arlotta, P., Fame, R.M., MacDonald, J.L., MacQuarrie, K.L., and Macklis, J.D. (2009). Novel subtype-specific genes identify distinct subpopulations of callosal projection neurons. *J. Neurosci.* 29, 12343–12354.
- Nieman, B.J., Lerch, J.P., Bock, N.A., Chen, X.J., Sled, J.G., and Henkelman, R.M. (2007). Mouse behavioral mutants have neuroimaging abnormalities. *Hum. Brain Mapp.* 28, 567–575.
- Nóbrega-Pereira, S., Gelman, D., Bartolini, G., Pla, R., Pierani, A., and Marín, O. (2010). Origin and molecular specification of globus pallidus neurons. *J. Neurosci.* 30, 2824–2834.
- Olsen, S.R., Bortone, D.S., Adesnik, H., and Scanziani, M. (2012). Gain control by layer six in cortical circuits of vision. *Nature* 483, 47–52.
- Pasca, S.P., Portmann, T., Voineagu, I., Yazawa, M., Shcheglovitov, A., Paşca, A.M., Cord, B., Palmer, T.D., Chikahisa, S., Nishino, S., et al. (2011). Using iPSC-derived neurons to uncover cellular phenotypes associated with Timothy syndrome. *Nat. Med.* 17, 1657–1662.
- Persico, A.M., and Bourgeron, T. (2006). Searching for ways out of the autism maze: genetic, epigenetic and environmental clues. *Trends Neurosci.* 29, 349–358.
- Sasaki, S., Tabata, H., Tachikawa, K., and Nakajima, K. (2008). The cortical subventricular zone-specific molecule Svet1 is part of the nuclear RNA coded by the putative netrin receptor gene *Unc5d* and is expressed in multipolar migrating cells. *Mol. Cell. Neurosci.* 38, 474–483.
- Seong, H.J., and Carter, A.G. (2012). D1 receptor modulation of action potential firing in a subpopulation of layer 5 pyramidal neurons in the prefrontal cortex. *J. Neurosci.* 32, 10516–10521.
- Shinawi, M., Liu, P., Kang, S.H., Shen, J., Belmont, J.W., Scott, D.A., Probst, F.J., Craigen, W.J., Graham, B.H., Pursley, A., et al. (2010). Recurrent reciprocal 16p11.2 rearrangements associated with global developmental delay, behavioural problems, dysmorphism, epilepsy, and abnormal head size. *J. Med. Genet.* 47, 332–341.
- Silverman, J.L., Turner, S.M., Barkan, C.L., Tolu, S.S., Saxena, R., Hung, A.Y., Sheng, M., and Crawley, J.N. (2011). Sociability and motor functions in Shank1 mutant mice. *Brain Res.* 1380, 120–137.
- Suter, D.M., Molina, N., Gatfield, D., Schneider, K., Schibler, U., and Naef, F. (2011). Mammalian genes are transcribed with widely different bursting kinetics. *Science* 332, 472–474.
- Takemoto, M., Hattori, Y., Zhao, H., Sato, H., Tamada, A., Sasaki, S., Nakajima, K., and Yamamoto, N. (2011). Laminar and areal expression of *unc5d* and its role in cortical cell survival. *Cereb. Cortex* 21, 1925–1934.
- Tang, S.H., Silva, F.J., Tsark, W.M., and Mann, J.R. (2002). A Cre/loxP-deleter transgenic line in mouse strain 129S1/SvImJ. *Genesis* 32, 199–202.
- Thurley, K., Senn, W., and Lüscher, H.R. (2008). Dopamine increases the gain of the input-output response of rat prefrontal pyramidal neurons. *J. Neurophysiol.* 99, 2985–2997.
- Wahlsten, D., Metten, P., and Crabbe, J.C. (2003). Survey of 21 inbred mouse strains in two laboratories reveals that BTBR T/+ *tf/tf* has severely reduced hippocampal commissure and absent corpus callosum. *Brain Res.* 971, 47–54.
- Ward, J.H. (1963). Hierarchical Grouping to Optimize an Objective Function. *J. Am. Stat. Assoc.* 58, 236.

- Weiss, L.A., Shen, Y., Korn, J.M., Arking, D.E., Miller, D.T., Fossdal, R., Saemundsen, E., Stefansson, H., Ferreira, M.A., Green, T., et al.; Autism Consortium (2008). Association between microdeletion and microduplication at 16p11.2 and autism. *N. Engl. J. Med.* *358*, 667–675.
- Yang, M., and Crawley, J.N. (2009). Simple behavioral assessment of mouse olfaction. *Curr. Protoc. Neurosci.* *8*, 8.24.
- Yang, M., Silverman, J.L., and Crawley, J.N. (2011). Automated three-chambered social approach task for mice. *Curr. Protoc. Neurosci.* *8*, 8.26.
- Yang, M., Bozdagi, O., Scattoni, M.L., Wöhr, M., Roulet, F.I., Katz, A.M., Abrams, D.N., Kalikhman, D., Simon, H., Woldeyohannes, L., et al. (2012). Reduced excitatory neurotransmission and mild autism-relevant phenotypes in adolescent Shank3 null mutant mice. *J. Neurosci.* *32*, 6525–6541.
- Yoo, A.S., Sun, A.X., Li, L., Shcheglovitov, A., Portmann, T., Li, Y., Lee-Messer, C., Dolmetsch, R.E., Tsien, R.W., and Crabtree, G.R. (2011). MicroRNA-mediated conversion of human fibroblasts to neurons. *Nature* *476*, 228–231.

Cell Reports, Volume 7

Supplemental Information

**Behavioral Abnormalities and Circuit Defects
in the Basal Ganglia of a Mouse Model
of 16p11.2 Deletion Syndrome**

Thomas Portmann, Mu Yang, Rong Mao, Georgia Panagiotakos, Jacob Ellegood, Gul Dolen, Patrick L. Bader, Brad A. Grueter, Carleton Goold, Elaine Fisher, Katherine Clifford, Pavitra Rengarajan, David Kalikhman, Darren Loureiro, Nay L. Saw, Zhou Zhengqui, Michael A. Miller, Jason P. Lerch, R. Mark Henkelman, Mehrdad Shamloo, Robert C. Malenka, Jacqueline N. Crawley, and Ricardo E. Dolmetsch

Supplementary Figure Legends

Figure S1. Targeting of the mouse chromosome 7F3 locus using two step homologous recombination, related to Figure 1. A) Detailed view of the 5' and 3' targeting constructs. DT-A: diphtheriatoxin A; CAG: chicken β -actin enhanced CMV promoter; *Neo^r*: neomycin resistance cassette; pA: poly A signal; STOP: translational stop codon (for all frames); *Puro^r*: puromycin resistance cassette; int: rabbit β -globin intron; *Che: mCherry*. B) The insertion site of the 5' LoxP site was shifted to the end of the *Coro1a* gene in order not to disrupt expression prior to recombination. Exons (dark grey boxes) are highlighted and numbered. C) Position of restriction sites and corresponding probes for southern blots (A: purple, B: green, C: orange). D) Position of primers for genotyping by PCR. Sequential recombination steps result in the deletion of 440kb containing the mouse homologues to the human chromosome 16p11.2 region. E- I) Verification of correct insertion of both targeting constructs using PCR (E and H) and Southern blot analysis (F, G and I) for one clone of the first targeting step and three independent clones after the second targeting step. Size and probe position for southern blotting are indicated in (C). For PCR primer positions refer to (D). J) *Cre-IresGFP* transfected mouse ESC colony (upper left) and untransfected control (lower right) 24 hours post transfection. K) Mouse ESC colonies for three independent clones imaged one passage post transfection showing mCherry expressing colonies after deletion of the *16p11* genes. L) *Cis* and *Trans* arrangements of the LoxP sites can lead to different outcomes with the *trans* arrangement allowing for duplication of one allele. M) Detection of the duplicated allele by PCR in a Cre-transfected mESC line with *trans* arrangement of the LoxP sites. N) Genotyping showing successful germline transmission of the floxed allele in F1 pups after crossing of chimeras with C57BL/6 females.

Figure S2. Single cell gene expression measurements, relates to Figure 3. A) Three representative genes showing lognormal distribution of single cell gene expression data for both wild type and *16p11^{+/-}* samples ($n > 1000$). Histograms show gene expression (X-axis: C_t) versus cell number (Y-axis) for *Rps18*, a ubiquitous/housekeeping gene; *Map2*, a pan-neuronal marker; and *Bola2*, a gene flanking the deleted region. B) Variance of gene expression across cells is shown as the

distance between the highest- and lowest-expressing cell for each gene. Note the log₂ scale for the horizontal axis reflecting a 10- to >1000-fold difference in expression of a gene across cells. C) Correlation of gene expression across cells for two housekeeping genes that are commonly used for normalization of total template input. Normalization on *Gapdh* and/or *Rps18* did not reduce the variance of gene expression across cells consistent with the low correlation of their expression across cells (across all >2000 cells, $r_{Gapdh/Rps18}=0.374$). D) Correlation of C_t for independent, non-alternatively spliced regions of the same ubiquitous transcript (*Cacna1c*) (4 brain regions, 1 array/region, n_{max}=92 cells per array). E) Reflection of gene expression changes in single cell data as seen for the *16p11* genes. Histograms reveal how allelic loss in *16p11*^{+/-} cells (+/-) affects the distribution of gene expression in comparison to wild type (+/+). F) Differential contribution of median expression level and detection frequency to gene expression changes. Shown are the median expression of each gene across cells (median expression/cell), the fraction of cells in which the transcript was detected (fraction of cells), as well as the calculated population average (population-based expression), which is the median expression/cell multiplied by fraction of cells expressing the gene (expected to be approximately 50% of wild type upon loss of one allele). Bars show *16p11*^{+/-} as a percentage of wild type. Left: Two representative genes also shown in A (*Map2*: 2 alleles in *16p11*^{+/-} cells) and D (*Mapk3*: 1 allele in *16p11*^{+/-} cells). Error bars indicate SEM across cells (for median expression per cell) or across animals (for the fraction of cells). Right: Averaged impact of allelic loss on median gene expression level and detection frequency over all *16p11* genes. Error bars depict SEM across genes (n=26). G) Detailed view of all *16p11* and four control genes. Note that for most of the *16p11* genes, the detection frequency (fraction of cells) is the more robust indicator of allelic loss than the median expression per cell. Some *16p11* genes are expressed in very few cells only thus showing a considerable SEM (compare also with B). H) Model for how loss of one allele is reflected in single cell gene expression data of the *16p11* genes. Average gene expression level per cell is indicated in black (100%) or grey (50%). Non-expressing cells are shown in white. Histograms are shown for bi-allelic (+/+, blue line) and mono-allelic (+/-, red line) condition. I) Co-expression map for subpallial cells generated by unsupervised clustering of FET p-values for pairs of genes.

Green: high co-expression frequency, red: low co-expression frequency (meaning high degree of mutual exclusiveness).

Figure S3. Gene expression changes as determined by single cell gene expression profiling *in vivo*, relates to Figure 4. Shown are significant ($p_{\text{FET}} < 0.005$) changes in population sizes between wild type (+/+) and $16p11^{+/-}$ (+/-) for A) subpallium, B) cortex, C) meso-diencephalon. The genes are listed in the order of statistical significance. The cutoff was defined based on the $16p11$ genes, which are expected to reflect an average 50% reduction in gene expression in $16p11^{+/-}$ samples and thus served as a general positive control for reflection of a 50% change in expression.

Figure S4. Callosal defects in juvenile $16p11^{+/-}$ mice, relates to Figure 4. A) Immunohistochemistry using an anti-SATB2 antibody to visualize callosal projection neurons in 20 μm cryo-sections of 1 week-old brains. B) Quantification of SATB2-positive cells (wild type n=3, $16p11^{+/-}$ n=3). C) Fractional Anisotropy (FA) differences of the corpus callosum suggesting either a loss in myelination, decreased axonal density, decreased axonal organization, or some combination thereof. In light of the relatively late onset of myelination in the corpus callosum of mice around P10, a myelination defect is less likely to contribute to the observed changes in white matter (Foran and Peterson, 1992). D) Voxel-wise FA difference in the male and female $16p11^{+/-}$ mouse compared to control, which localizes the FA differences. E-G) highlight that corpus callosum differences in the $16p11^{+/-}$ mouse are more severe in the females than males. Errorbars represent SEM. * indicates $q < 0.05$ and ** $q < 0.01$.

Figure S5. Independent confirmation of $Drd1^+$ and $Drd2^+$ cell population abnormalities in the juvenile $16p11.2$ mouse model by Horev and colleagues, relates to Figures 4 and 5. A) Coronal sections showing the expression of $Drd2\text{-GFP}$ and $Drd1\text{-tdTomato}$ BAC transgenes in the $16p11.2^{df/+}$ (Horev et al., 2011) and wild-type background at age P7. Yellow frames indicate regions shown in B-D. TdTomato⁺ cells populate distinct cortical regions at varying density, potentially reflecting a differential

need for dopaminergic modulation in functionally distinct cortical subdomains. B) Zoom in to dorsolateral striatum and deeper-layer somatosensory cortex show excess numbers of GFP⁺ cells (*Drd2*⁺) in striatum and reduced numbers of tdTomato⁺ cells (*Drd1*⁺) in cortex of *16p11.2^{df/+}* compared to wild type. C) Fewer *Drd1*⁺ cells are also detected in medial cortical regions of *16p11.2^{df/+}* mice. D) Detailed view of striatum around the anterior commissure again shows the increase GFP⁺ cells in the *16p11.2^{df/+}* brain, while the pattern of tdTomato⁺ cells appears comparable to wild type. E) Quantification of GFP⁺ cells corroborate the increase GFP⁺ cells in the *16p11.2^{df/+}* striatum ($p=0.031$). Errorbars represent SEM. * indicates $p<0.05$

Figure S6. Various behaviors of *16p11^{+/-}* mice, relates to Figure 7. Animal ages: adult (2-3 months, A-I), juvenile (P21-P25, J). A) Forelimb grip strength normalized by body weight did not differ significantly between the *16p11^{+/-}* and wild-type groups ($t_{45}=1.19$, NS for tests done at SBFNL; $F_{1,24} = 3.81$, NS, and Table S3 for tests done at NIMH). B) Both genotypes showed normal olfactory habituation and dishabituation responses to sequential presentations of water, two non-social odors, and two social odors. Habituation was significant for both genotypes on three consecutive trials of water presentations, *16p11^{+/+}*, $p<0.01$; *16p11^{+/-}*, $p<0.01$. Dishabituation was significant for both genotypes on water to almond: *16p11^{+/+}*, $p<0.01$; *16p11^{+/-}*, $p<0.01$. Habituation to almond, *16p11^{+/+}*, $p<0.01$; *16p11^{+/-}*, $p<0.01$. Dishabituation almond to banana: *16p11^{+/+}*, $p<0.01$; *16p11^{+/-}*, $p<0.05$. Habituation to banana, *16p11^{+/+}*, $p<0.01$; *16p11^{+/-}*, $p<0.01$. Dishabituation banana to social odor 1: *16p11^{+/+}*, $p<0.01$; *16p11^{+/-}*, $p<0.01$. Habituation to social odor 1, *16p11^{+/+}*, $p<0.01$; *16p11^{+/-}*, $p<0.01$. Dishabituation social odor 1 to social odor 2: *16p11^{+/+}*, $p<0.05$; *16p11^{+/-}*, $p<0.01$. Habituation to social odor 2, *16p11^{+/+}*, $p<0.01$; *16p11^{+/-}*, $p<0.01$. C) Rotarod performance of adult animals (2-3 months): No significant genotype differences were detected in mice tested on an accelerating rotarod (4-40 rpm, $F_{1,25}=0.09$, NS) (C) or at 24 rpm (D), or at accelerating 0-40 rpm (data not shown). On the accelerating rotarod, *16p11^{+/-}* mice were tested for 2 trials per day for 3 consecutive days and their latency to fall from the rod was recorded. The interval between the two trials on the same day was 1 hour. At 24 rpm, adult *16p11^{+/-}* mice and their wild-type littermates underwent six 5-min trials over the course

of two days, with three trials on each day; the average latency per day (mean \pm SEM) was presented. No significant genotype differences were found on rotarod performance

E) No significant genotype differences in self-grooming were found in males ($F_{1,23}=1.67$, NS) or females ($F_{1,22}=0.028$, NS). F) The $16p11^{+/-}$ mice showed similar time spent in the center versus the periphery in an open field ($t_{86}=1.243$, NS), suggesting no increased anxiety compared to wild type. G) Poor swimming abilities in many of the $16p11^{+/-}$ mice prevented cognitive testing on the Morris water maze. Cut off latency = 60s. H) To determine whether there are any defects in the working memory of $16p11^{+/-}$ mice, we tested these mice on a Y maze spontaneous alternation task. The $16p11^{+/-}$ mice performed indistinguishably from their wild-type littermates on this task: the percentages of alternations were similar between these groups ($t_{89}=0.68$, NS), and are higher than the 50% chance level of alternation. I) To assess spatial working/episodic-like learning and memory in adult $16p11^{+/-}$ mice, we tested these mice on a modified Barnes maze task, also known as a delayed-matching-to-place (DMP) task, which excludes the water and swimming factors by using a dry maze. The $16p11^{+/-}$ mice exhibited similar acquisition of the task to their wild-type littermates, as measured by their averaged escape latencies (Trial 1-2 savings: $t_{21}=0.44$, NS; Trial 1-4 savings: $t_{21}=1.90$, NS) over the course of five days (four trials per day).

J) Juvenile (age P21-P25) reciprocal social interaction: In Cohort 1 males ($16p11^{+/+}$ $n=10$, $16p11^{+/-}$ $n=13$), no significant genotype differences were found on nose-to-nose sniff ($F_{1,21}=3.28$, NS), front approach ($F_{1,21}=2.84$, NS), anogenital sniff ($F_{1,21}=0.02$, NS), follow ($F_{1,21}=2.17$, NS), arena exploration ($F_{1,21}=0.56$, NS), and self-grooming ($F_{1,21}=0.43$, NS). $16p11^{+/-}$ males exhibited significantly more push-crawls as compared to wildtype littermates ($F_{1,21}=4.45$, $p<0.05$). In Cohort 1 females ($16p11^{+/+}$ $n=11$, $16p11^{+/-}$ $n=13$), no significant genotype differences were found on nose-to-nose sniff ($F_{1,22}=0.11$, NS), front approach ($F_{1,22}=0.24$, NS), anogenital sniff ($F_{1,22}=0.91$, NS), follow ($F_{1,22}=0.02$, NS), push-crawl ($F_{1,22}=0.08$, NS), and arena exploration ($F_{1,22}=0.07$, NS). $16p11^{+/-}$ females exhibited significantly fewer bouts of self-grooming as compared to wildtype littermates ($F_{1,21}=11.72$, $p<0.01$). Similar results were found in Cohort 2. In Cohort 2 males ($16p11^{+/+}$ $n=12$, $16p11^{+/-}$ $n=10$), no significant genotype differences were found on nose-to-nose sniff ($F_{1,20}=1.92$, NS), front approach ($F_{1,20}=0.66$, NS),

follow ($F_{1,20}=2.21$, NS), arena exploration ($F_{1,20}=2.66$, NS), and self-grooming ($F_{1,20}=0.14$, NS). $16p11^{+/-}$ males exhibited significantly more anogenital sniffs ($F_{1,20}=10.29$, $p<0.01$) and more push-crawls ($F_{1,20}=12.15$, $p<0.01$) as compared to wildtype littermates. In Cohort 2 females ($16p11^{+/+}$ $n=12$, $16p11^{+/-}$ $n=10$), no significant genotype differences were found on nose-to-nose sniff ($F_{1,20}=0.63$, NS), front approach ($F_{1,20}=1.32$, NS), anogenital sniff ($F_{1,20}=0.04$, NS), follow ($F_{1,20}=2.66$, NS), push-crawl ($F_{1,20}=0.43$, NS), arena exploration ($F_{1,20}=0.32$, NS), and self-grooming ($F_{1,20}=2.66$, NS). Panel 6B, 6C, 6E, 6G, 6J: NIMH, panel 6A, 6D, 6F, 6H-I: SBFNL.

Figure S7. Adult social interaction, relates to Figure 7. Normal sociability was observed in multiple cohorts of adult (2-3 months) mice of both genotypes at NIMH and at SBFNL. A-H) In a standard 3-chambered social approach test, in Cohort 1, both genotypes spent significantly more time in the chamber containing the novel mouse than in the chamber containing the novel object, and more time sniffing the novel mouse than the novel object. *Chamber time*: male $16p11^{+/+}$, $F_{1,10}=28.67$, $p<0.001$; male $16p11^{+/-}$, $F_{1,11}=24.22$, $p<0.001$; female $16p11^{+/+}$, $F_{1,8}=48.85$, $p<0.001$; female $16p11^{+/-}$, $F_{1,9}=44.55$, $p<0.001$; *Sniff time*: male $16p11^{+/+}$, $F_{1,10}=71.97$, $p<0.001$; male $16p11^{+/-}$, $F_{1,11}=21.19$, $p<0.001$; female $16p11^{+/+}$, $F_{1,8}=59.58$, $p<0.001$; female $16p11^{+/-}$, $F_{1,9}=44.96$, $p<0.001$. Similarly, both genotypes of Cohort 2 displayed normal sociability. *Chamber time*: male $16p11^{+/+}$, $F_{1,9}=20.16$, $p<0.01$; male $16p11^{+/-}$, $F_{1,9}=81.18$, $p<0.001$; female $16p11^{+/+}$, $F_{1,10}=8.36$, $p<0.05$; female $16p11^{+/-}$, $F_{1,10}=23.73$, $p<0.001$; *Sniff time*: male $16p11^{+/+}$, $F_{1,9}=34.98$, $p<0.001$; male $16p11^{+/-}$, $F_{1,9}=157.56$, $p<0.001$; female $16p11^{+/+}$, $F_{1,10}=21.59$, $p<0.001$; female $16p11^{+/-}$, $F_{1,10}=37.95$, $p<0.001$. I-P) In the three-chambered social approach tasks performed at SBFNL, adult $16p11^{+/-}$ mice in both sexes showed significant sociability as well as preference for social novelty, as indicated by significantly more time spent in the chamber containing the novel mouse than in the chamber containing the novel object (sociability test) or the familiar mouse (social novelty test), and also by the significantly more time spent sniffing the novel mouse than the novel object (sociability test) or the familiar mouse (social novelty test).). For sociability test, *chamber time*: male $16p11^{+/+}$, $t_{33}=5.52$, $p<0.001$; male $16p11^{+/-}$, $t_{19}=6.81$, $p<0.001$; female $16p11^{+/+}$, $t_{28}=6.88$, $p<0.001$; female $16p11^{+/-}$, $t_{20}=5.43$, $p<0.001$; *sniff time*: male $16p11^{+/+}$, $t_{33}=5.38$, $p<0.001$; male $16p11^{+/-}$, $t_{19}=6.34$, $p<0.001$;

female $16p11^{+/+}$, $t_{28}=8.39$, $p<0.001$; female $16p11^{+/-}$, $t_{20}=6.63$, $p<0.001$. For social novelty test, *chamber time*: male $16p11^{+/+}$, $t_{34}=1.00$, NS; male $16p11^{+/-}$, $t_{20}=2.41$, $p<0.001$; female $16p11^{+/+}$, $t_{26}=4.58$, $p<0.001$; female $16p11^{+/-}$, $t_{40}=3.45$, $p<0.01$; *sniff time*: male $16p11^{+/+}$, $t_{35}=1.22$, NS; male $16p11^{+/-}$, $t_{20}=3.35$, $p<0.01$; female $16p11^{+/+}$, $t_{26}=3.75$, $p<0.001$; female $16p11^{+/-}$, $t_{20}=3.05$, $p<0.01$. For all statistical significance: *, $p<0.05$; **, $p<0.01$; ***, $p<0.001$. Panel 5A-H: NIMH, panel I-P: SBFNL.

Table S1. DNA oligonucleotide primers for genotyping and southern blot analysis. Oligonucleotides are shown 5' to 3'

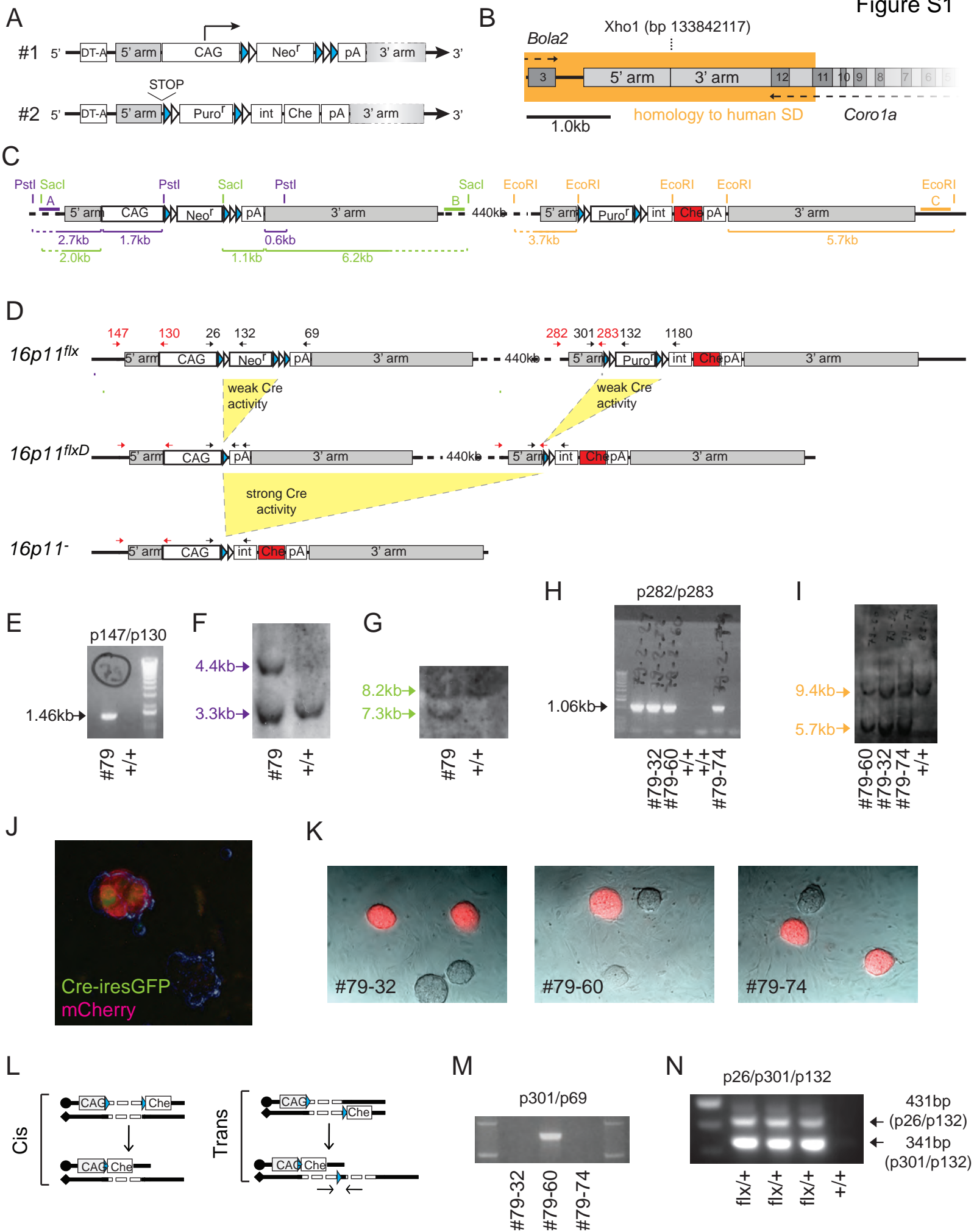
Table S2. DNA oligonucleotide primers for single cell multiplex qPCR experiments. Oligonucleotides are shown 5' to 3'

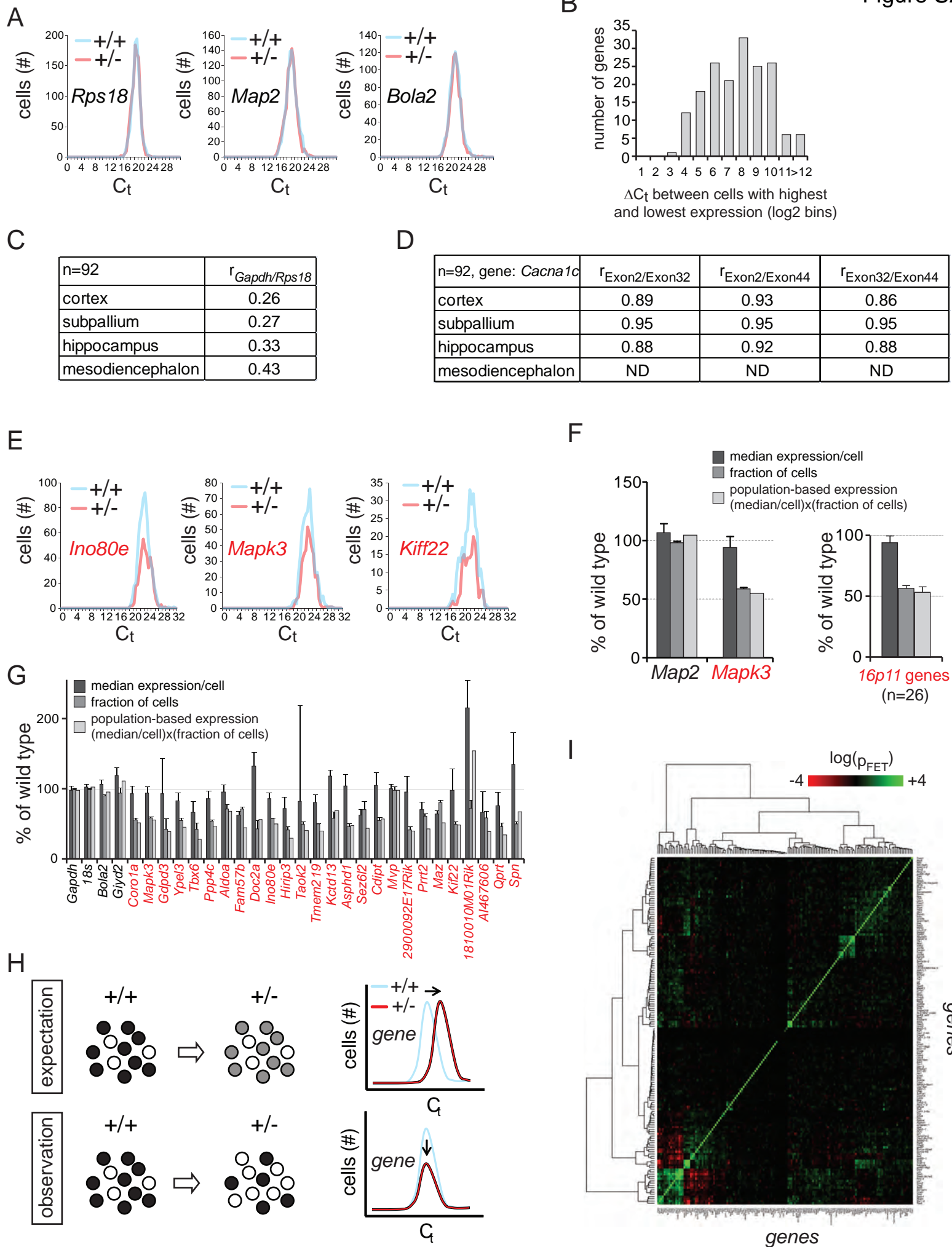
Table S3. General health as assessed at NIMH. Adult mice were evaluated for general health and neurological reflexes between 2-3 months of age. No physical abnormalities or deficits in simple reflexes were detected in $16p11^{+/-}$ mice. The only effect of genotype was on body weight, with $16p11^{+/-}$ mice weighing significantly less than wild-type controls ($p<0.05$). No balding patches were observed in mice evaluated during this age range. Observations of home cage behaviors revealed no abnormalities in general activity, group huddling, and nesting. No excessive aggressive behaviors were observed in adult males.

Table S4. General health assessed by SBFNL. The adult $16p11^{+/-}$ mice ($n=36$) displayed specific changes in their general health and behavioral traits during the SHIRPA primary screen compared to their littermate controls ($n=52$), as measured in the viewing jar, in the arena, and above the arena. Both male and female mice are included in the screen. All values for the wild type and $16p11^{+/-}$ groups are reported as percentage of the population. The p values were calculated from χ^2 test: *, $p < 0.05$; **, $p < 0.01$; ***, $p < 0.001$; NS, not significant.).

Movie S1. Defects in gait and motor control of juvenile $16p11^{+/-}$ mice. $16p11^{+/-}$ pups recorded at P10 are hyperactive, show tremor, tumbling and difficulty in motor control compared to wild-type litter mates.

Horev, G., Ellegood, J., Lerch, J.P., Son, Y.E., Muthuswamy, L., Vogel, H., Krieger, A.M., Buja, A., Henkelman, R.M., Wigler, M., *et al.* (2011). Dosage-dependent phenotypes in models of 16p11.2 lesions found in autism. *Proc Natl Acad Sci U S A* *108*, 17076-17081.





A

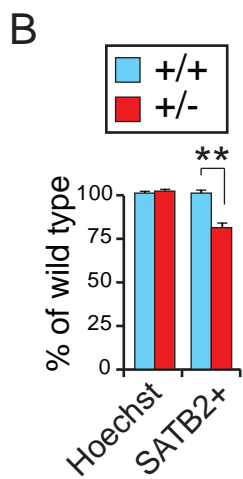
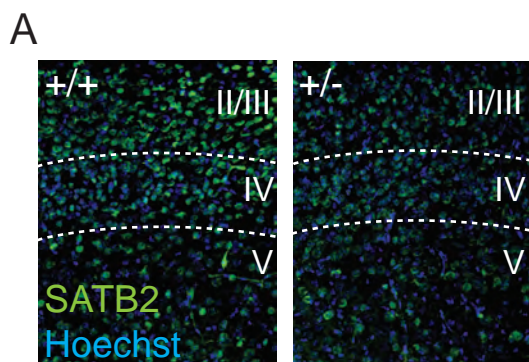
subpallium	p (FET)	+/- (%)	SEM	+/- (%)	SEM	change (%)
<i>Hirip3</i>	2.E-08	28.9	(+/- 4.6)	11.8	(+/- 2.4)	-59.2
<i>Foxp1</i>	3.E-07	69.6	(+/- 8.5)	86.4	(+/- 6.6)	24.1
<i>Ino80e</i>	3.E-07	53.5	(+/- 5)	34.4	(+/- 1.9)	-35.8
<i>Ctip2</i>	3.E-06	71.9	(+/- 2.4)	86.4	(+/- 3.4)	20.2
<i>Maz</i>	7.E-06	78.2	(+/- 3.4)	62.9	(+/- 5.4)	-19.6
<i>Ppp4c</i>	1.E-04	34.3	(+/- 3.2)	20.8	(+/- 1.6)	-39.4
<i>Fam57b</i>	1.E-04	62.5	(+/- 3.9)	45.6	(+/- 3.5)	-27.0
<i>Reelin</i>	1.E-04	18.9	(+/- 10.1)	32.4	(+/- 9.5)	71.1
<i>Asphd1</i>	2.E-04	28.5	(+/- 4)	16.4	(+/- 2.8)	-42.2
<i>Robo1</i>	3.E-04	48.7	(+/- 4.5)	63.0	(+/- 6.3)	29.5
<i>Prrt2</i>	3.E-04	35.3	(+/- 2)	23.1	(+/- 2.4)	-34.7
<i>Kif22</i>	4.E-04	26.7	(+/- 1.6)	15.6	(+/- 1.7)	-41.5
<i>Gdpd3</i>	0.001	5.1	(+/- 0.7)	0.9	(+/- 0.6)	-82.0
<i>Plxnd1</i>	0.001	18.8	(+/- 2.6)	29.8	(+/- 6.1)	58.4
<i>Penk</i>	0.002	14.2	(+/- 7.4)	26.0	(+/- 10.6)	83.4
<i>Drd2</i>	0.003	25.7	(+/- 2.0)	38.0	(+/- 2.0)	47.3
<i>Cdipt</i>	0.003	12.6	(+/- 2)	5.8	(+/- 2)	-53.5
<i>Aldoa</i>	0.003	45.2	(+/- 8.7)	34.5	(+/- 8.7)	-23.7
<i>Sez6l2</i>	0.003	54.9	(+/- 1.2)	41.8	(+/- 5.6)	-23.8
<i>Nfh-Nefh</i>	0.005	5.6	(+/- 0.7)	11.8	(+/- 2.5)	111.7
<i>Adora2a</i>	0.005	28.0	(+/- 1.7)	40.1	(+/- 2.7)	43.0

B

cortex	p (FET)	+/- (%)	SEM	+/- (%)	SEM	change (%)
<i>Ino80e</i>	2.E-15	67.3	(+/- 2.7)	36.9	(+/- 3.5)	-45.2
<i>Prrt2</i>	2.E-12	48.5	(+/- 3.1)	22.6	(+/- 3.3)	-53.5
<i>Reelin</i>	4.E-12	42.3	(+/- 11.9)	16.9	(+/- 4.6)	-60.0
<i>Somatostatin</i>	3.E-10	30.6	(+/- 11.7)	10.3	(+/- 2.1)	-66.3
<i>Fam57b</i>	6.E-10	76.6	(+/- 4.6)	49.6	(+/- 5.8)	-35.2
<i>Kctd13</i>	4.E-09	36.9	(+/- 2.5)	17.2	(+/- 4.3)	-53.4
<i>MapK3</i>	5.E-09	57.7	(+/- 3.2)	35.4	(+/- 6.7)	-38.7
<i>Doc2a</i>	3.E-08	18.7	(+/- 5.8)	5.0	(+/- 1.7)	-73.4
<i>Npy</i>	8.E-08	61.5	(+/- 12.8)	39.7	(+/- 12.2)	-35.5
<i>Kif22</i>	1.E-07	32.4	(+/- 3.2)	15.0	(+/- 2.8)	-53.7
<i>Asphd1</i>	4.E-07	34.6	(+/- 1.4)	17.7	(+/- 4.4)	-48.9
<i>Sez6l2</i>	5.E-07	65.3	(+/- 1.3)	43.0	(+/- 6.2)	-34.2
<i>Tmem219</i>	6.E-07	36.5	(+/- 1.1)	19.4	(+/- 4.5)	-46.8
<i>Drd1</i>	1.E-06	31.1	(+/- 3.5)	13.0	(+/- 3.1)	-58.2
<i>S100a10</i>	2.E-06	40.1	(+/- 6.2)	22.4	(+/- 5.7)	-44.1
<i>Lpl</i>	7.E-06	23.2	(+/- 3.7)	10.0	(+/- 2.5)	-56.9
<i>Aldoa</i>	7.E-06	68.6	(+/- 2.7)	51.4	(+/- 6.1)	-25.1
<i>Maz</i>	7.E-06	78.4	(+/- 3.7)	62.4	(+/- 5)	-20.5
<i>Ypel3</i>	8.E-06	36.2	(+/- 3.5)	20.2	(+/- 1.7)	-44.1
<i>Hirip3</i>	1.E-05	28.5	(+/- 2.0)	14.7	(+/- 3.5)	-48.6
<i>Mef2c</i>	1.E-05	49.7	(+/- 17.3)	31.1	(+/- 14.6)	-37.6
<i>Ppp4c</i>	3.E-05	41.9	(+/- 5.1)	26.1	(+/- 1.8)	-37.6
<i>Tle4</i>	7.E-05	75.5	(+/- 8.8)	60.1	(+/- 9.9)	-20.4
<i>Slc1a3</i>	8.E-05	65.5	(+/- 7.5)	49.9	(+/- 6.3)	-23.8
<i>Darpp32</i>	9.E-05	19.3	(+/- 5)	8.6	(+/- 2.1)	-55.6
<i>Taok2</i>	1.E-04	40.2	(+/- 14.6)	25.5	(+/- 8.6)	-36.6
<i>Neo1</i>	2.E-04	37.7	(+/- 3.4)	39.3	(+/- 4.1)	4.2
<i>Pax6</i>	2.E-04	42.7	(+/- 4.7)	28.7	(+/- 6)	-32.9
<i>bola2</i>	3.E-04	86.1	(+/- 1.4)	74.7	(+/- 2.3)	-13.2
<i>Bex4</i>	3.E-04	85.7	(+/- 4.7)	74.2	(+/- 4.6)	-13.5
<i>Src</i>	4.E-04	93.3	(+/- 0.6)	82.9	(+/- 4.2)	-11.2
<i>Akt1</i>	6.E-04	92.3	(+/- 1.1)	81.8	(+/- 6.6)	-11.4
<i>Coro1A</i>	6.E-04	29.6	(+/- 3.2)	18.0	(+/- 2.7)	-39.2
<i>Arnt2</i>	8.E-04	10.5	(+/- 12.1)	3.3	(+/- 2.8)	-68.1
<i>Foxp1</i>	9.E-04	67.2	(+/- 9.9)	53.4	(+/- 7.6)	-20.4
<i>Nr4a3</i>	9.E-04	27.9	(+/- 2)	16.9	(+/- 4)	-39.4
<i>Ntsr1</i>	0.001	21.4	(+/- 3.9)	11.9	(+/- 2.1)	-44.1
<i>Kitl</i>	0.001	29.9	(+/- 6.5)	18.2	(+/- 4.9)	-39.1
<i>Pcp4</i>	0.001	59.8	(+/- 7)	46.5	(+/- 4.7)	-22.3
<i>Ntf3</i>	0.002	16.6	(+/- 1.6)	8.3	(+/- 1)	-49.7
<i>Kcnj6</i>	0.002	11.5	(+/- 2.5)	5.0	(+/- 1)	-56.5
<i>Dkk3</i>	0.002	42.0	(+/- 5.8)	30.1	(+/- 4.4)	-28.3
<i>Sox5</i>	0.002	79.6	(+/- 4.2)	68.6	(+/- 1.4)	-13.8
<i>Map2</i>	0.003	97.9	(+/- 0.7)	93.1	(+/- 2.8)	-4.9
<i>Cntn6</i>	0.003	35.1	(+/- 3.2)	24.5	(+/- 2.6)	-30.4
<i>Rheb</i>	0.004	53.4	(+/- 4.5)	41.0	(+/- 6.2)	-23.2

C

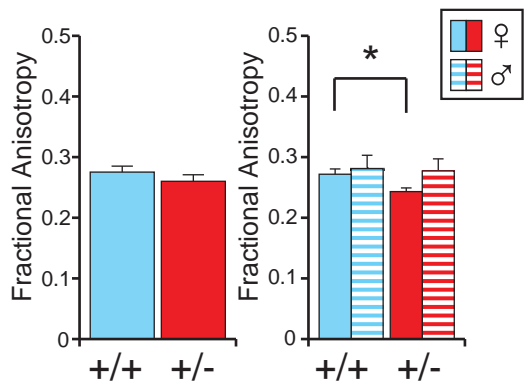
meso-diencephalon	p (FET)	+/- (%)	SEM	+/- (%)	SEM	change (%)
<i>Sez6l2</i>	7.E-10	72.3	(+/- 4.7)	45.6	(+/- 9.7)	-37.0
<i>Aldoa</i>	3.E-09	87.2	(+/- 3.3)	64.8	(+/- 3.8)	-25.7
<i>Fam57b</i>	8.E-09	70.3	(+/- 3.5)	45.4	(+/- 5.6)	-35.5
<i>Ppp4c</i>	5.E-08	51.3	(+/- 3.4)	27.2	(+/- 3.1)	-47.0
<i>MapK3</i>	6.E-08	64.4	(+/- 3.7)	40.4	(+/- 3.7)	-37.3
<i>Tmem219</i>	9.E-07	36.6	(+/- 2.1)	17.1	(+/- 3.4)	-53.3
<i>Maz</i>	1.E-06	79.5	(+/- 2.1)	59.4	(+/- 2.3)	-25.3
<i>Ino80e</i>	3.E-06	65.4	(+/- 2.1)	44.2	(+/- 3.3)	-32.4
<i>Prrt2</i>	7.E-06	68.4	(+/- 5.4)	48.7	(+/- 1.3)	-28.8
<i>Taok2</i>	1.E-05	19.5	(+/- 5.3)	6.5	(+/- 1.7)	-66.7
<i>Coro1A</i>	2.E-05	30.8	(+/- 3.1)	14.8	(+/- 2.9)	-52.0
<i>Kctd13</i>	5.E-05	36.0	(+/- 5.8)	19.6	(+/- 2.3)	-45.5
<i>Cdipt</i>	7.E-05	32.7	(+/- 2.5)	17.1	(+/- 0.5)	-47.7
<i>Robo2</i>	1.E-04	20.0	(+/- 5.8)	7.7	(+/- 0.3)	-61.4
<i>Kif22</i>	2.E-04	25.2	(+/- 6.9)	12.2	(+/- 1.7)	-51.8
<i>Ypel3</i>	2.E-04	33.6	(+/- 1.8)	18.6	(+/- 0.9)	-44.5
<i>Foxp2</i>	3.E-04	78.3	(+/- 3.6)	63.5	(+/- 10.5)	-18.9
<i>Scn1a</i>	3.E-04	44.6	(+/- 4)	28.8	(+/- 0.9)	-35.3
<i>Kitl</i>	4.E-04	79.2	(+/- 2.3)	65.6	(+/- 8.1)	-17.2
<i>Th</i>	0.001	20.7	(+/- 2.4)	9.9	(+/- 2.9)	-52.0
<i>Zic1</i>	0.001	48.1	(+/- 1.9)	33.6	(+/- 6.8)	-30.1
<i>Asphd1</i>	0.002	28.8	(+/- 3.9)	16.6	(+/- 0.6)	-42.2
<i>Sult1a1</i>	0.002	22.7	(+/- 2.4)	12.0	(+/- 3.8)	-47.0
<i>Doc2a</i>	0.002	23.5	(+/- 2.8)	12.5	(+/- 5.1)	-46.8
<i>Otx2</i>	0.003	53.8	(+/- 2.9)	40.4	(+/- 6.9)	-24.8
<i>Drd1</i>	0.003	17.8	(+/- 2.7)	8.5	(+/- 1)	-52.3
<i>Cux1</i>	0.003	17.8	(+/- 1.4)	8.6	(+/- 1)	-51.8
<i>Gad65</i>	0.004	1.7	(+/- 0.8)	7.2	(+/- 4.7)	333.7
<i>S100a10</i>	0.005	50.0	(+/- 4.4)	37.9	(+/- 5)	-24.2



C

Corpus Callosum

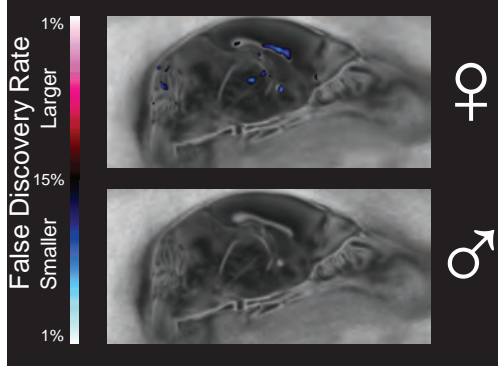
Fractional Anisotropy Differences

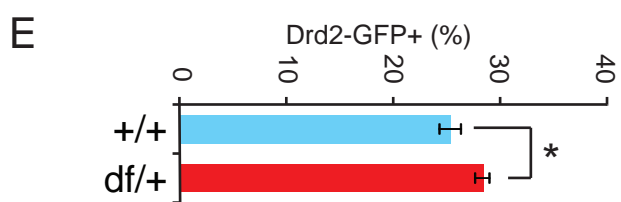
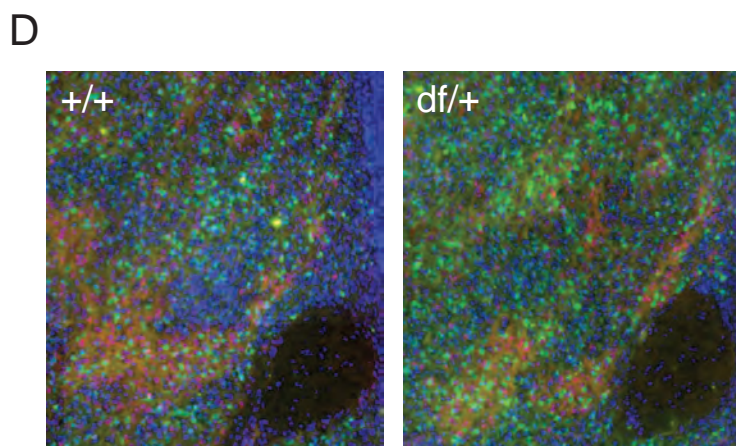
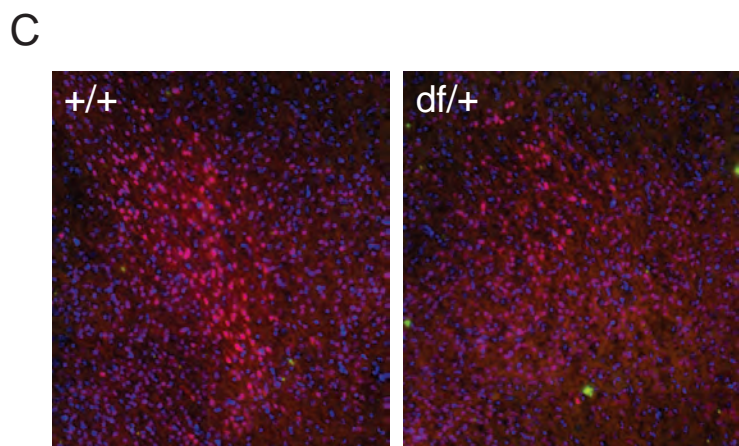
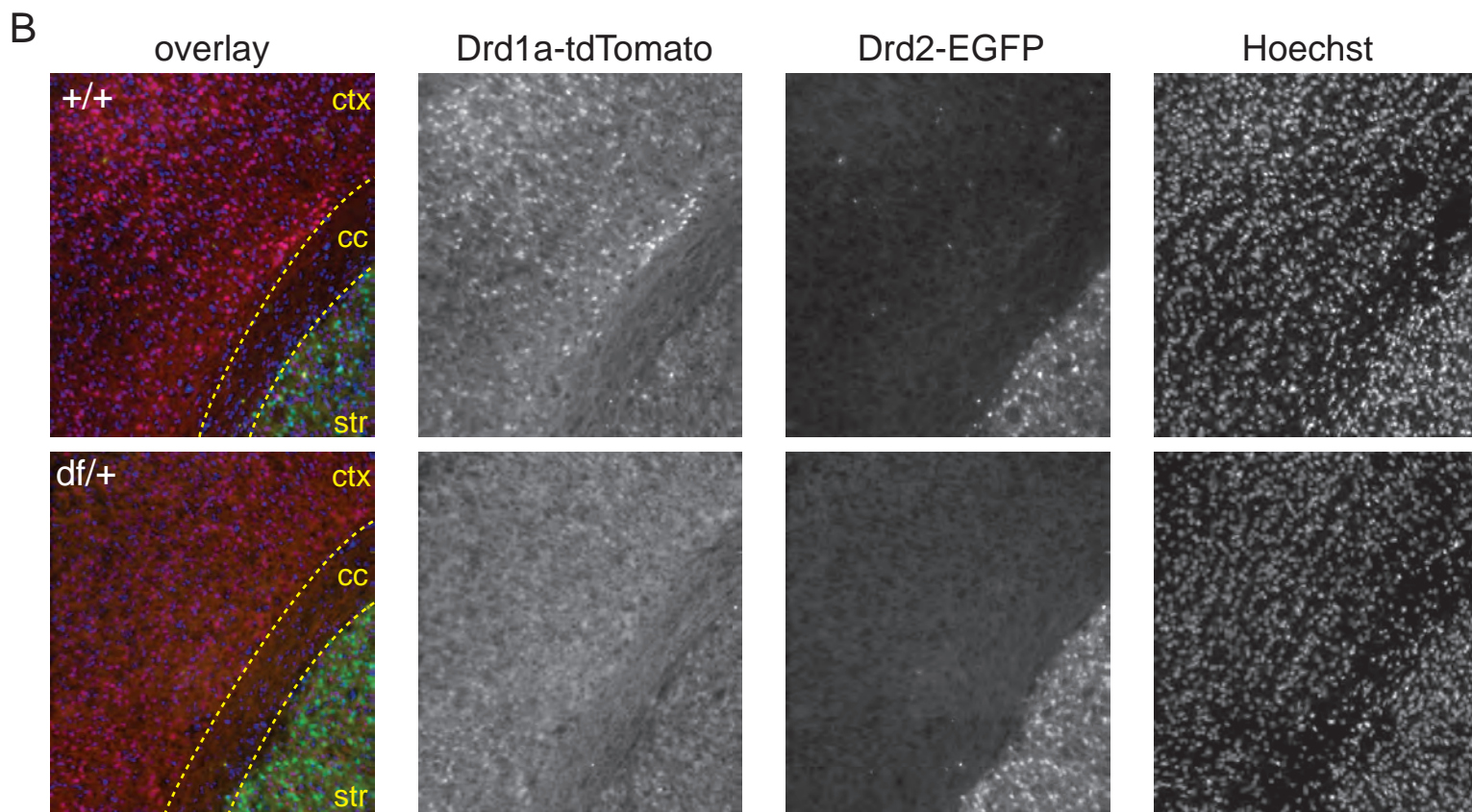
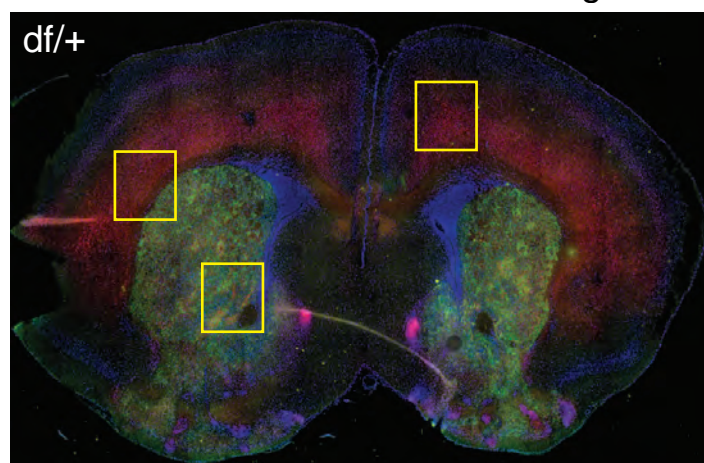
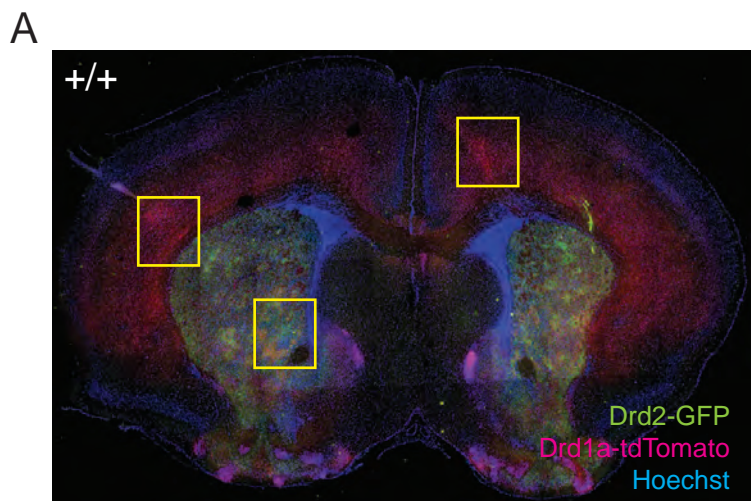


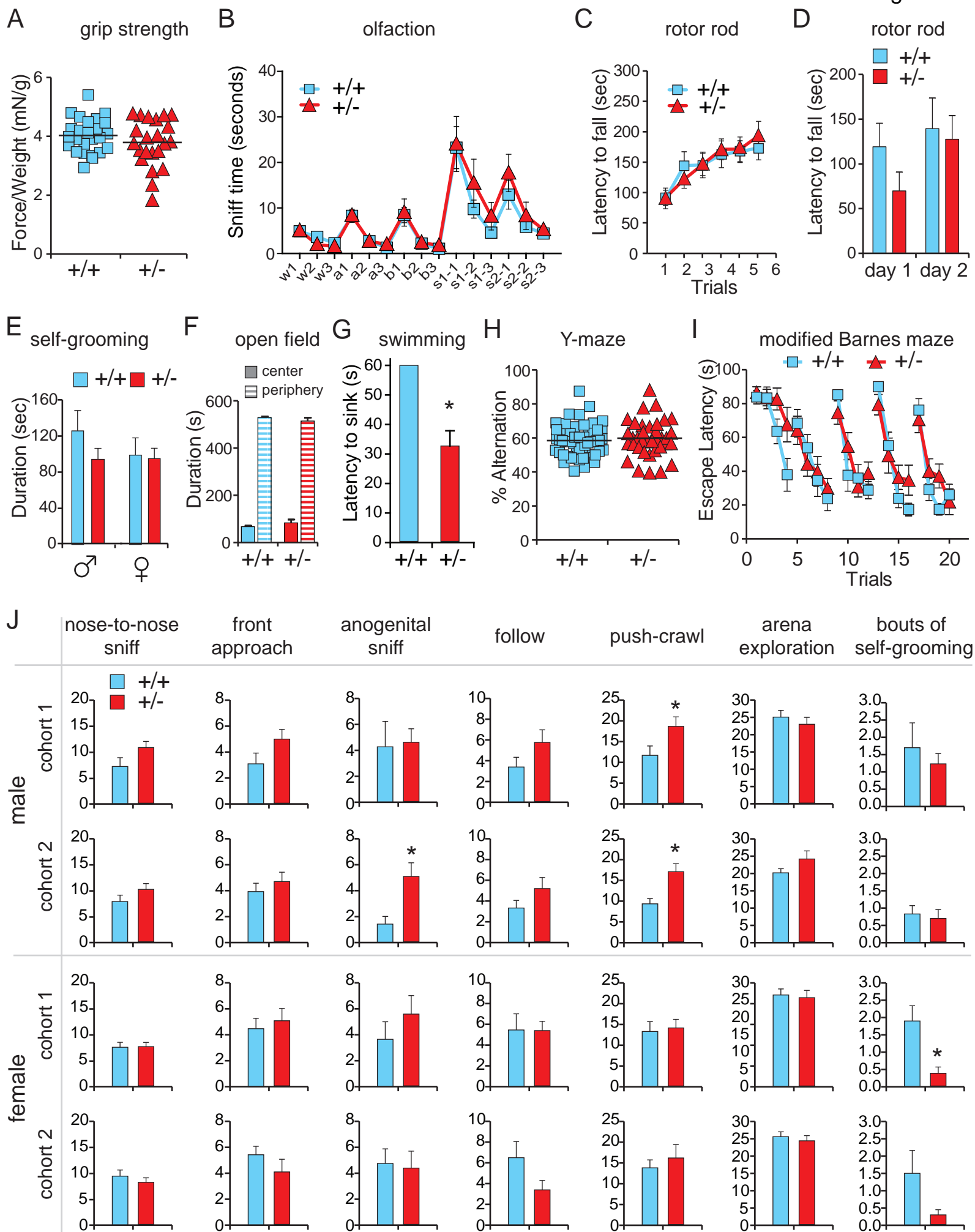
D

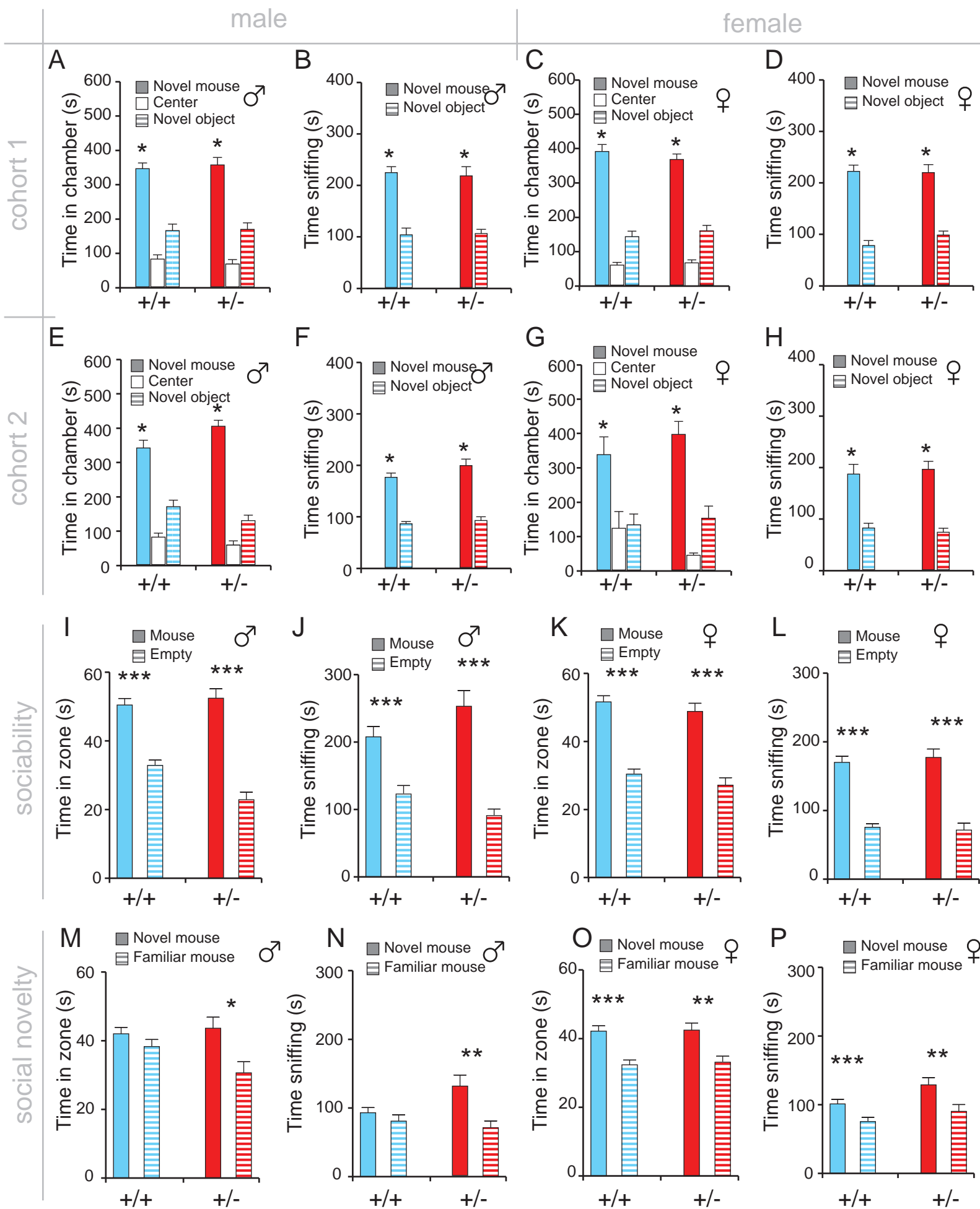
16p11 +/- vs +/+

Fractional Anisotropy Differences









Southern probes	forward primer	reverse primer
probe A	CTTGATTTTCATCACAGAGGTTGGT	GCCCTCCTCTCTTCAGCACACCCAT
probe B	CTTCGTGCTGGGACTCCAGTCCT	GCAAGTAGGTCCCAGAGTGCTC
probe C	GGAGGTGATTGAGAGGACAGAGG	CTTGCTACCCAGGTCCATTCTAC

Genotyping	sequence	direction
p26	TTCGGCTTCTGGCGTGTGAC	forward
p69	CCGCTCGAGGGATCCGCGTCGAGGGATCTCC	reverse
p130	GCGTACTATGGGAACATACGTCAT	reverse
p132	GGTGGATGTGGAATGTGTGCGAG	reverse
p147	CTTGATTTTCATCACAGAGGTTGGT	forward
p282	TCTCAGCCAGCTCAGCTATATC	forward
p283	TGCAGGAATTCGATATCTACTTAG	reverse
p301	TTGGACAGACCCTGGTTCAGTC	forward
p1180	CATGGTGATACAAGGGACATCTTC	reverse

General health and neurological screening of 16p11+/- mice

Genotypes	WT (N=15)	HET (N=15)	P value
Fur condition (3 pt scale)	2	2	NS
Bald patches (%)	0	0	NS
Missing whiskers (%)	0	0	NS
Piloerection (%)	0	0	NS
Body tone (3 pt scale)	2	2	NS
Limb tone (3 pt scale)	2	2	NS
Physical abnormalities (%)	0	0	NS
Body weight (grams)	28.6±1.9	23.8±1.40	p<.05
Body Temperature (°C)	31.8±.07	31.8±.24	NS
Empty cage behavior			
Transfer freezing (%)	0	0	NS
Wild running (%)	0	0	NS
Sterotypies (%)	0	0	NS
Exploration (3 pt scale)	2	2	NS
Motoric abilities			
Trunk curl (%)	100	100	NS
Wire hang (latency sec)	60	60	NS
Grip Strength (force)	157±5.5	141±6.2	NS
Reflexes			
Forepaw reach (%)	100	100	NS
Righting reflex (%)	100	100	NS
Corneal (%)	100	100	NS
Pinna (%)	100	100	NS
Vibrissae (%)	100	100	NS
Reactivity			
Struggle/vocalization (%)	0	0	NS
Dowel biting (3 pt scale)	1	1	

Table S4

Test		+/+	+/-	P value
Behavior recorded in the viewing jar				
Body position	Inactive	0	13.9	
	Active	96.2	80.6	*
	Excessive activity	3.8	5.6	
Tremor	Present	0	19.4	***
Palpebral closure	Eyes open	100	94.4	
	Eyes closed	0	5.6	NS
Coat appearance	Tidy and well-groomed	100	100	
	Irregularities	0	0	NS
Whiskers	Present	100	100	NS
Lacrimation	Present	0	11.1	*
Defecation	Present	76.9	55.6	*
Behavior recorded in the arena				
Transfer arousal	Extended freeze	1.9	13.9	
	Brief freeze	82.7	66.7	NS
	Immediate movement	15.4	19.4	
Gait	Fluid movement	80.8	47.2	
	Lack of fluidity in movement	19.2	52.8	***
Tail elevation	Dragging	2.0	2.9	
	Horizontal extension	86.3	70.6	NS
	Elevated/straub tail	11.8	26.5	
Startle response	None	26.9	72.2	
	Preyer reflex	26.9	19.4	**

	Other reaction	46.2	8.3	
Touch escape	No response	3.8	11.1	
	Responds to touch	67.3	69.4	NS
	Flees prior to touch	28.8	19.4	
Behavior recorded above the arena				
Positional passivity	Struggles when held by tail	46.2	44.4	
	Struggles when held by neck	13.5	5.6	
	Struggles when laid supine	34.6	44.4	NS
	No struggle	5.8	5.6	
Trunk curl	Present	48.1	88.9	***
Limb grasping	Present	1.9	11.1	NS
Pinna reflex	Present	53.8	58.3	NS
Corneal reflex	Present	100	88.9	*
Contact righting reflex	Present	94.2	69.4	**
Evidence of biting	None	71.2	88.9	
	Biting in response to handling	28.8	11.1	*
Vocalization	None	50	75	
	Vocal	50	25	***
Visual reaching	No response until face touches	4	22.7	
	Reach when vibrissae touch	56	63.6	NS
	Reach from far away	40	13.6	

Supplementary Experimental Procedures

Targeting of the *16p11* genes

The overall targeting strategy included sequential targeting with two targeting vectors (Figure S1A). The LoxP sites were positioned as close to the human break points as technically possible (Figure 1A, Figure S1B). The insertion sites for the LoxP sites were chosen based on the most common 16p11.2 CNV associated with ASD (Figure 1A; (Weiss et al., 2008)). According to this CNV, non-homologous recombination involving the segmental duplications on either end of the region is thought to result in a breakpoint in exon 11 of *CORO1A*, removing the gene upstream of this exon in the case of the deletion. Targeting of the mouse *Coro1a* gene and inserting a LoxP site at the corresponding position (chr7:133843812) would have disrupted the gene already within the floxed *16p11* allele (*16p11^{flx}*). We therefore moved the position of the LoxP site to an Xho1 restriction site (chr7:133842117), which is 1165bp downstream of the last exon of *Coro1a*. On the opposite end of the *16p11* region, the synteny between human 16p11.2 and mouse 7F3 ends upstream of the *Spn* gene, due to lack of the segmental duplication in mouse. Targeting vector #2 therefore inserted the LoxP site on chr7:134285222, 3336 bp upstream of *Spn*. A fluorescent reporter gene (*mCherry*) was included to allow for the detection of deletion of the locus *in vivo* (Figure 1D, Figure S1A, J, K). 129/OLA mouse embryonic stem cells were sequentially targeted by electroporation with the linearized targeting constructs. For each targeting step, clones were analysed by PCR and Southern blot analyses (Figure S1E-I). Primers for PCR genotyping and Southern probes are listed in Table S1. Positive clones were injected into C57BL/6N blastocysts at the Stanford Transgenic Mouse Research Facility. The sequential targeting of DNA constructs resulted in both *cis* and *trans* arrangements of the LoxP sites in different mESC clones, as verified by PCR analysis of *Cre*-transfected ESC clones (Figure S1L-M). Three mESC clones (two *cis*, one *trans*) were injected into C57BL/6N blastocysts to generate chimeric mice. Germ line transmission was successful only for the *cis* arrangement, and animals were bred to a ubiquitous *HPRT-Cre^{tg}* mouse line (Tang et al., 2002). In male offspring, transmission of the *HPRT-Cre^{tg}* and *16p11^{flx}* alleles therefore resulted in heterozygous deletion for the

$16p11$ genes ($16p11^{+/-}$). Due to the location of the $HPRT-Cre^{tg}$ transgene on the X chromosome transmission of $HPRT-Cre^{tg}$ and $16p11^{flx}$ alleles in female offspring resulted in mosaic animals carrying $16p11^{+/-}$ cells, as well as cells which carried the floxed allele lacking the Neo^r and $Puro^r$ ($16p11^{flx\Delta/+}$) genes. Removal of the selection markers was likely due to remaining Cre activity from the oocyte and zygote prior to X-inactivation.

In vitro analysis of the $16p11$ deletion

MESCs were transfected with a $pCAG-Cre-IRES-EGFP$ plasmid using Lipofectamine 2000 (Invitrogen) according to the manufacturer's recommendations and cells were examined for mCherry protein expression after 20 hours and one passage later.

Animals, housing and breeding at Stanford University

Mice were housed in pathogen-free and light- and temperature-controlled conditions. Food and water were available *ad libitum*. All animal experiments were in accordance with the APLAC protocols by Stanford. Chimeric mice were crossed with $HPRT-Cre^{tg/+}$ transgenic mice of mixed C57BL/6N and CD1 background. Furthermore, chimeric animals were bred to C57BL/6N females to maintain $16p11^{flx/+}$ mice. For $16p11^{+/-}$ mice, all further generations were bred with $16p11^{+/-}$ males and C57BL/6N females for back breeding onto C57BL/6N background.

General anatomical analyses

Body weight was measured at various time points ($n \geq 6$ for all time periods indicated) and normalized on the average weight of gender-matched, wild-type littermates. Adult (20 week) body length was measured from nose tip to tail root and normalized on average body length of gender-matched wild-type mice. Brain weight was measured post-fixation (4% PFA, at P7), including olfactory bulbs.

Food intake measurements

Food intake measurements were adapted from Kern et al. (Kern et al., 2012). Mice were kept without food (water *ad libitum*) for 16 hours prior to measurements. Body and food

weight were measured at the beginning of each measurement period. After 24 hours, animals and remaining food were weighed again and the amount of food eaten during the past 24-hour period was calculated. Food intake over 4 consecutive measurement periods was averaged for each animal before calculating the genotype average.

MRI study

Image Acquisition

The contrast required for registration and assessment of volume is not acceptable with our typical T2-weighted imaging sequence. We choose to use Diffusion Tensor Imaging (DTI) to enhance the contrast between white and gray matter to aid in the registration and volume measurements. This has the added benefit of allowing for diffusion measurements, such as fractional anisotropy, in addition to the volume measurements.

Diffusion Tensor Imaging Sequence

The DTI sequence uses an in-house custom built 3-coil solenoid array to acquire images from 3 brains in parallel (Nieman et al., 2007). The DTI scanning used a 6-cm inner bore diameter insert gradient, which was required for the increased gradient strength needed in the DTI sequence design. The DTI sequence used was a 3D diffusion-weighted FSE, with TR= 350 ms, echo train length = 6, first TE = 30 ms, TE = 6 ms for the remaining 5 echoes, one average, FOV = 25 mm × 14 mm × 14 mm, and a matrix size of 324 × 180 × 180, which yielded an image with 78 μm isotropic voxels. Five initial $b=0$ s/mm² images were acquired and 30 high b-value ($b = 1917$ s/mm²) in 30 different directions corresponding to the Jones30 scheme (Jones et al., 1999). Total imaging time was ~ 15 hours.

Registration and Analysis

To visualize and compare the mouse brains for the anatomical volume assessment the 30 high b-value images were averaged together to make a high contrast image necessary for accurate registration. Then these images were linearly (6 parameter followed by a 12 parameter) and nonlinearly registered together. All scans were then resampled with the appropriate transform and averaged to create a population atlas representing the average anatomy of the study sample. All registrations were performed

using a combination of the mni_autoreg tools (Collins et al., 1994) and ANTS (Avants et al., 2011). The result of the registration was to have all scans deformed into exact alignment with each other in an unbiased fashion. For the volume measurements, this allowed for the analysis of the deformations needed to take each individual mouse's anatomy into this final atlas space, the goal being to model how the deformation fields relate to genotype (Lau et al., 2008; Nieman et al., 2006). The Jacobian determinants of the deformation fields are then calculated as measures of volume at each voxel. For the diffusion measurements, the images were analyzed using the FSL software package (FMRIB, Oxford UK), which was used to create Fractional Anisotropy (FA) maps for each of the 52 brains used in this study. Then the same transformation that was used on the averaged high b-value images was applied to the FA maps to align them. The intensity differences can then be calculated between genotypes. Structures of interest were segmented based upon a pre-classified atlas (Dorr et al., 2008) and were assessed in all brains. Further, these measurements were examined on a voxel-wise basis in order to localize the differences found within regions or across the brain. Multiple comparisons were controlled for by using the False Discovery Rate (FDR) (Genovese et al., 2002).

96.96 Dynamic Arrays and sc-qPCR

Neonate brain tissues were incubated with Papain solution for 5 minutes at room temperature followed by the addition of inhibitor solution and gentle trituration. FACS was performed at the Stanford Shared FACS Facility. Gating for exclusion of debris and multiplets, as well as dead cells (propidium-iodide+) was identical for all samples and brain regions. 96.96 dynamic array (Fluidigm Inc., CA) experiments were performed as previously described and according to the recommended protocol by the array manufacturer. Single-cell cDNA samples were included for further analysis based on expression of both *Rps18* and *Gapdh* genes.

Sc-qPCR data analysis

1) *Variability of gene expression levels*: Consistent with earlier studies, we found that single-cell gene expression showed a lognormal distribution in our experiments (Figure S2A; (Bengtsson et al., 2005). The average standard deviation of expression of a gene

(n=172 genes expressed in at least 3% of cells) over all cells (n>2000) and experiments was 1.73 PCR cycles, and the difference between the lowest and highest expressing cell was 7.93 PCR cycles for the average gene. Consistent with the heterogeneity of our cell populations, this result was higher than that previously reported for homogenous cell populations and may also be influenced by the types of genes examined (Figure S2B; compare to: “Application Guidance: Single-Cell Data Analysis”, #100-5066, Fluidigm Inc., CA; available at <http://www.fluidigm.com/single-cell-guidance-request.html> by Fluidigm Inc.). To test whether this variance across cells was due to a technical artifact we used three primer pairs targeting the same transcript (*Cacna1c*, at exons 2, 32, and 44; Figure S2D). The expression of the *Cacna1c* gene as measured by these independent primer pairs was highly correlated ($r>0.85$) across all single cells, suggesting that the observed variability is not due to the reverse transcription or the amplification of the cDNA but reflects bona fide biological variation.

2) *Data normalization across cells*: In population-based gene expression profiling by qPCR, normalization using “housekeeping” genes is necessary to correct for varying mRNA input levels. Housekeeping genes are chosen based on their near perfect correlation with input mRNA under various experimental conditions (e.g., *Gapd*, *Rps18*). For technical reasons, in a single cell, we cannot measure total mRNA levels. However, we can measure the correlation of different housekeeping genes across cells and test whether the normalization of single-cell data using these genes reduces the variance (thus, normalizing for common parameters introducing variance, such as total mRNA content of a cell). We failed to find a strong correlation between the expression of the commonly used housekeeping genes *Rps18* and *Gapdh* at the single-cell level ($r<0.5$ in all samples tested per brain region; $r=0.374$ over all >2000 single cells across brain regions, Figure S2C). In contrast, when we analyzed the C_t for primer pairs targeting independent sites of the same, ubiquitously-expressed transcript (*Cacna1c*: exons 2, 32 and 44), we observed a strong correlation of $r>0.85$ throughout the data sets tested (Figure S2D), suggesting that technical noise, such as different primer efficiencies or biased pre-amplification, are unlikely to account for the high variability of gene expression across cells and the low correlation of two common housekeeping genes. Consequently, normalization using either *Gapdh* and/or *Rps18* did not narrow the

variance across cells (standard deviation of the average gene when normalized on *Gapdh*: 1.85, on *Rps18*: 1.73). This finding is in contrast to what is observed in population-based qPCR that averages thousands of cells, but is consistent with models of bursting gene transcription and consequential fluctuations in mRNA levels across time.

3) *Gene expression changes*: Overall, our genetic mouse model caused a 50% population-based reduction in the 26 *16p11* genes (Figure 1 D). However, given the variability of gene expression across cells (Figure S2B) it was unclear how this would be reflected in single-cell gene expression. We expected that there might be a shift in the median expression across cells by one PCR cycle (equaling 50% less template). However (Figure S2 E-H), single-cell analysis of the 26 *16p11* genes revealed that removal of one allele in *16p11*^{+/-} mice did not result in hugely decreased median expression levels of the *16p11* genes across cells (-6.2%, $p_{\text{TTEST}}=0.381$ n.s., $n_{\text{genes}}=26$). Instead, we observed a major decrease in the fraction of cells that express a specific *16p11* gene (-43.4%, $p_{\text{TTEST}}=0.013$). The population average of *16p11* genes in *16p11*^{+/-} cells, which is the product of these two numbers, ends up close to the expected 50% of wild type expression (53.1%, or a change of -46.9%, compare also Figure S2F with Figure 1D)). Our observations indicate that in single cells the gene expression change associated with removal of one allele is, to a considerable extent, reflected in an altered detection frequency, rather than the median expression across cells (see also model in Figure S2H). This is consistent with current models of transcriptional kinetics as it could be a consequence of a decreased rate of transcriptional bursts due to loss of one copy of a gene, which would increase the chance that an mRNA is not detected at a specific time (Chubb et al., 2006; Raj et al., 2006; Suter et al., 2011). It is further of critical importance in the light of data interpretation and detection of gene expression changes in single cell data sets, and has to our knowledge not been previously reported.

4) *False positive/negative results*: False positives resulting from nonspecific primer binding can be identified using information available from the melting curve. In addition, contamination by the two genomic DNA templates in each single-cell sample is unlikely, since, whenever technically possible, we selected primers across exons that would result in different melting temperatures for products synthesized from cDNA and

genomic DNA. We did not observe melting curves matching genomic DNA-derived products for any gene (data not shown). In light of models for bursting transcriptional kinetics at the single-allele level, we cannot exclude the possibility that we might fail to detect transcripts in some cells, although the gene locus was considered active in this cell type if averaged over time. Such apparent false negative results could occur as a result of harvesting a cell during down-time in the transcriptional cycle as opposed to during (or right after) the last transcriptional burst.

Example for co-expression mapping

Co-expression mapping was based on p values derived from Fisher's Exact Test (p_{FET}). Fisher's exact test has several advantages for assessment of co-expression of genes because (1) it calculates an exact significance of a deviation from the null hypothesis (random expression of two genes), in contrast to an approximation that becomes exact towards an infinite sample size. Therefore (2), it out-performs similar tests, such as the Chi-square test, at small sample sizes while still being valid for large sample sizes, and (3) it allows for reaching smaller p values if genes are expressed in small populations of cells, thus increasing the resolution of subsequent clustering for smaller subpopulations of cells. The p values were then converted to their logarithm $\log(p_{FET})$ to center values around zero and buffer for extreme p values for genes expressed in only a few cells. To further account for the latter effect, a cutoff was introduced and genes were only included if they were expressed by at least 3% of total cells.

The following is an example of co-expression mapping based on our data for two genes specifically expressed in the inhibitory subpopulation of the neonate mouse cortex (n=504), *Gad67* and *Gad65*:

Co-expression table:

cells (#)	<i>Gad67</i>	<i>Gad65</i>
<i>Gad67</i>	72	54
<i>Gad65</i>	54	105

2x2 contingency table:

co-expression	yes	no	row total
observed (Fo)	54	450	504
expected (Fe)	15	489	504
column total	69	939	1008

For this example, the $p_{FET} = 1.17E-06$, the logarithm, $\log(p_{FET}) = -5.93$. Re-introducing an algebraic sign (- for $Fo > Fe$; + for $Fo < Fe$) reveals that the p value applies to an increased degree of co-expression for the gene pair *Gad67* and *Gad65*. The following table shows the top eight p_{FET} , $\log(p_{FET})$, algebraic sign and cluster input for the *Gad67* gene:

	$p_{FET}(Gad67)$	$\log(p_{FET})$		algebraic sign	cluster input
<i>Gad67</i>	1.31E-13	-12.88	Fo>Fe	-	12.88
<i>Gad65</i>	1.17E-06	-5.93	Fo>Fe	-	5.93
<i>Dlx5</i>	1.45E-06	-5.84	Fo>Fe	-	5.84
<i>Vgat</i>	4.57E-04	-3.34	Fo>Fe	-	3.34
<i>Dlx1</i>	2.04E-03	-2.69	Fo>Fe	-	2.69
<i>Unc5d</i>	4.14E-03	-2.38	Fo<Fe	+	-2.38
<i>Emx1</i>	1.83E-02	-1.74	Fo<Fe	+	-1.74
<i>NeuroD1</i>	2.56E-02	-1.59	Fo<Fe	+	-1.59

As expected, *Gad67* shows the highest degree of co-expression with itself. In addition, expression of the next 7 genes reveals that *Gad67* expression distinguishes cortical inhibitory neurons expressing the known markers *Gad67*, *Gad67*, *Dlx5*, *Vgat*, and *Dlx1* (green) from cortical excitatory neurons expressing *Unc5d*, *Emx1*, and *Neurod1* (red). In conclusion, the method not only allows for identifying gene modules specific to cell types, but also an unbiased assessment of expression pattern specificity of a gene.

Immunohistochemistry

The following primary antibodies were used in combination with Alexa-488 and Alexa-647 coupled goat secondary antibodies: mouse anti-SATB2 (Abcam, #ab51502), chicken anti-GFP (Abcam, #ab13970), rabbit anti-DARPP32 (Cell Signaling Technology, #2302S), rat anti-CTIP2 (Abcam, #18465), guinea pig anti D1R (Frontier

Institute Co.Ltd, #D1R-GP-Af500).

Spine analysis

300 μ m coronal sections were prepared on a standard microtome and mounted on glass slides. Golgi staining was performed using the FD Rapid GolgiStain Kit (FD NeuroTechnologies, Inc.) according to the manufacturer's recommendations. Bright-field image stacks were taken at 0.2 μ m intervals using a Zeiss AxioImager microscope. 10 medium spiny neurons per genotype were identified based on their characteristic morphology and 5-10 primary dendrites were traced and analyzed using Neurolucida Software.

Electrophysiology

Parasagittal slices (250 μ m) containing the NAc core were prepared from wild-type and *16p11^{+/-}* mice on a C57BL/6N background (postnatal days 28–56). Briefly, after mice were killed with isoflurane, brains were quickly removed and placed in ice-cold, low sodium, high sucrose dissecting solution. Slices were cut by adhering the two sagittal hemispheres of brain containing the NAc core to the stage of a Leica vibroslicer. Slices were allowed to recover for a minimum of 60 min. in a submerged holding chamber (~25°C) containing artificial cerebrospinal fluid (ACSF) consisting of 124 mM NaCl, 4.4 mM KCl, 2.5 mM CaCl₂, 1.3 mM MgSO₄, 1 mM NaH₂PO₄, 11 mM glucose and 26 mM NaHCO₃. Slices were then removed from the holding chamber and placed in the recording chamber where they were continuously perfused with oxygenated (95% O₂, 5% CO₂) ACSF at a rate of 2 ml per min. at 30 \pm 2°C. Picrotoxin (50 μ M) was added to the ACSF to block GABAA receptor-mediated inhibitory synaptic currents. Whole-cell voltage-clamp recordings from MSN were obtained using IR-DIC video microscopy. The NAc core was identified by the presence of the anterior commissure. Recordings were made with electrodes (3.0–6.0 M Ω) filled with 120 mM CsMeSO₄, 15 mM CsCl, 8 mM NaCl, 10 mM HEPES, 0.2 mM EGTA, 10 mM TEA-Cl, 4 mM Mg²⁺ATP, 0.3 mM

Na²⁺GTP, 0.1 mM spermine and 5 mM QX-314. Excitatory afferents were stimulated with a bipolar nichrome wire electrode placed at the border between the NAc core and cortex dorsal to the anterior commissure. Recordings were performed using an Axopatch 1D or Multiclamp 700B (Molecular Devices), filtered at 2 kHz and digitized at 10 kHz. EPSCs of 100–400 pA were evoked at a frequency of 0.1 Hz while MSN were voltage-clamped at –70 mV unless otherwise stated. Data acquisition and analysis were performed on-line using custom Igor Pro software. Input resistance and access resistance were monitored continuously throughout each experiment; experiments were terminated if these changed by >20%. Paired-pulse ratios (PPR) were acquired by applying a second afferent stimulus of equal intensity at a specified time after the first stimulus and then calculating EPSC1/EPSC2. For a given ISI for each cell, the PPRs of six consecutive responses were averaged. NMDAR:AMPA ratios were calculated as the ratio of the magnitude of the EPSC recorded at +40 mV at 50 ms after afferent stimulation (NMDAR EPSCs) to the peak amplitude of the EPSC at –80 mV (AMPA EPSCs). Miniature EPSCs were collected at a holding potential of –70 mV in the presence of 500 nM TTX. Ten-second blocks of events were acquired and analyzed using Mini-analysis software (Synaptosoft) with threshold parameters set at 5 pA amplitude and <3 ms rise time. All events included in the final data analysis were verified by eye. Comparisons between different experimental manipulations were made using a two-tailed Student's *t*-test with *p*<0.05 considered significant. All statements in the text regarding differences between grouped data indicate that statistical significance was achieved. All values are reported as mean ± s.e.m.

Behavioral Assays at the Stanford Behavioral and Functional Neuroscience Laboratory, SBFNL

16p11^{+/-} and wild-type mice, all age-matched at the time of testing, were maintained on a C57BL/6N background, after backcrossing with C57BL/6N wild-type mice (Charles River) for 5-7 generations. In many tests, pure C57BL/6N mice were used as an additional control group to ensure the proper design and execution of these tests (data

not shown). Mouse colonies were maintained at the SBFNL in accordance with National Institutes of Health and Stanford guidelines for care and use of laboratory animals. Behavioral assays reported here were performed by investigators who were blind to the genotypes of the mice. We tested four cohorts of adult mice (aged 2–9 months), including males and females, in the order from the least to the most aversive tests to minimize the potential for previous experience to influence, possibly in a genotype-dependent manner, behavioral phenotypes on subsequent tests. Mice were maintained in a 12-hour reverse light/dark cycle. With the exception of tests requiring daylight conditions (open field), all behavioral testing was performed during the dark cycle. The experimenters habituated all animals for 3–5 sessions (~10 min. in each session, once a day) prior to the day of the first experiment. In these habituation sessions, mice were acclimated to handling by the experimenter. The experimenter wore gloves, habituated the mice to handling by allowing them to walk or run from hand to hand, until the mice showed no apparent signs of stress or fear. The investigators were blind to the genotypes. Experimental conditions were counterbalanced by genotype.

Data were presented as mean \pm SEM. Chi-square tests were used for determining statistical significance in a standardized, comprehensive behavioral primary screen, the **SmithKline Beecham, Harwell, Imperial College, Royal London Hospital Phenotype Assessment (SHIRPA)**. Where appropriate, either Student's *t*-test or the repeated measures two-way ANOVA, was used for statistical analysis in the home cage activity, activity chamber, open field, grip strength, startle response, six-trial novel object recognition, Y maze, modified Barnes maze, three-chamber social approach tasks, and activity chamber with risperidone treatment tests. The Bonferroni test was used for post-hoc analysis. In all statistical analyses, normal distribution of the data was tested using the D'Agostino and Pearson omnibus normality test.

SHIRPA, home cage behavioral monitoring (5-day habituation prior to 4-hr monitoring), activity chamber (10 min.), open field (10 min.), grip strength, rotarod, startle response (40ms of 110dB pulse, 10s ITI), Y maze spontaneous alternation task, modified Barnes maze and three-chamber sociability and social novelty tasks were performed according

to previously established protocols at the SBFNL (Bader et al., 2011; Faizi et al., 2012; Faizi et al., 2011; Ishizaki et al., 2010).

Motor coordination

Motor coordination and function was assessed with a ROTOR-ROD™ (San Diego Instrument). Mice were tested at either accelerating 0-40 rpm or constant 24 rpm over 5 min. Two animals were tested concurrently in separate 11.4 cm-wide lanes on a rod with a diameter of 3.2 cm. Three trials were performed on each testing day after one day of training. Animals received, at minimum, 30 min. of rest between trials. For each trial, the latency to fall from the rod was recorded.

Novel object recognition

A novel object recognition task, which is based on the innate tendency of mice to differentially explore a novel stimulus over a familiar one (reviewed in (Antunes and Biala, 2012)), was repeated in six trials to evaluate the memory of *16p11^{+/-}* mice in recognizing a previously presented object. During testing, single-housed subject mice were presented with an object in a home cage environment in a total of six 1-min. trials with ITIs of 10 min. In trials 1–4, mice were exposed to the same object that had been presented as a novel object in trial 1. In the fifth trial, subject mice were presented with a second novel object. In the sixth trial, mice were presented with the first object. Trials were videotaped for subsequent manual scoring of sniffing time on the object by an experimenter blinded to the genotypes.

Behavioral assays at NIMH

Twelve *16p11^{+/+}* females and six *16p11^{+/-}* males were transferred from Stanford University in Palo Alto, CA to the National Institute of Mental Health Intramural Research Program in Bethesda, MD, where two cohorts of offspring were generated and behaviorally tested. To avoid confounds of changes in maternal behaviors, all subjects were generated by mating *16p11^{+/+}* females and *16p11^{+/-}* males. Mice were weaned at three weeks of age, and group housed by sex in cages of 2-4 littermates per cage. To improve pup survival (up to 60% of the Mendelian ratio), breeding cages were supplemented with high-fat rodent chow and fresh fruit. Further, *16p11^{+/-}* pups received

a concentrated liquid dietary supplement (Stat®, Pegasus Laboratories, Pensacola, FL) and vitamin B12 injection were used to treat underweight $16p11^{+/-}$ pups in several cases. In cases where wild-type pups outnumbered $16p11^{+/-}$ pups, extra wild-type pups were culled to reduce competition. All weanlings were provided with fresh fruit supplements until 4 weeks of age. To healthy adults, standard rodent chow and tap water were available *ad libitum*. Underweight adults were provided with dietary supplements. In addition to standard bedding, a Nestlet square and a cardboard tube (Jonesville Paper Tube Corp., MI, USA) were provided in each cage. The colony room was maintained on a 12:12 light/dark cycle with lights on at 7:00 AM with temperature maintained at approximately 20°C and humidity kept at 55%. All experiments were conducted between 9:00 AM and 5:00 PM. All procedures were approved by the National Institute of Mental Health Animal Care and Use Committee.

Pup body weight

A subset of were weighed on postnatal day 6, as previously described (Scattoni et al., 2008; Yang et al., 2012).

Juvenile reciprocal social interaction

Juvenile reciprocal social interactions were tested between 21 and 25 days of age. The test was conducted in the Noldus PhenoTyper Observer 3000 chamber (Noldus, Leesburg, Virginia) as previously described (Briellmaier et al., 2012; Chadman et al., 2008; Ey et al., 2012; Yang et al., 2012). The floor of the arena was covered with a 0.5 cm layer of clean bedding. Each subject mouse was singly housed in a clean cage for one hour before the test. After this brief isolation period, the freely moving subject mouse and a freely moving age- and sex-matched B6 partner mouse were simultaneously placed in the arena and their interactions were videotaped for 10 min. Social interactions were scored by a highly trained observer, using Noldus Observer 5.0 software. Parameters of social behaviors included nose-to-nose sniff, front approach, follow, nose-to-anogenital sniff, and push-crawl. Besides social behaviors, non-social arena exploration and bouts of self-grooming were scored as measures of exploratory activity and repetitive behavior, respectively. All behaviors were analyzed for frequency of occurrence, i.e. number of bouts.

Automated three-chambered social approach task

Social approach was assayed in our automated three-chambered apparatus (NIMH Research Services Branch, Bethesda, MD) as previously described (Briemaier et al., 2012; Chadman et al., 2008; Silverman et al., 2011; Yang et al., 2012; Yang et al., 2011). Novel target mice were 129S1/SvImJ mice between 8 and 16 weeks of age, of the same sex as the subjects. The apparatus was a rectangular, three-chambered box made of clear polycarbonate. Retractable doorways built into the two dividing walls controlled access to the side chambers. Number of entries and time spent in each chamber were automatically detected by photocells embedded in the doorways and tallied by the software. The test session began with a 10 min habituation session in the center chamber only, followed by a 10 min habituation in all three empty chambers. The subject was then briefly confined to the center chamber while the clean novel object (an inverted stainless steel wire pencil cup, Galaxy, Kitchen Plus, <http://www.kitchen-plus.com>) was placed in one of the side chambers. A novel mouse was placed in an identical wire cup located in the other side chamber. A disposable plastic drinking cup containing a lead weight was placed on the top of each inverted wire pencil cup to prevent the subject from climbing on top. The sides containing the novel object and the novel mouse alternated between the left and right chambers across subjects. After both stimuli were positioned, the two side doors were simultaneously lifted and the subject was allowed access to all three chambers for 10 min. Time spent in each chamber and entries into each chamber were automatically tallied. Time spent sniffing the novel object and time spent sniffing the novel mouse during the 10 min test session were later scored from video recordings, by an observer using two stopwatches. The apparatus was cleaned with 70% ethanol and water between subjects. Up to four subject mice were tested in the same room at the same time, using a high-throughput multi-unit arrangement of the 4 test chambers.

General health and neurological reflexes

Measures of general health and neurological reflexes were evaluated in adult mice as previously described (Briemaier et al., 2012; Silverman et al., 2011; Yang et al., 2012). General health was assessed by fur condition, whisker condition, body weight, body temperature, body and limb tone. Neurological reflexes were assessed by forepaw reaching, righting reflex, trunk curl, whisker twitch, pinna response, eyeblink response

and auditory startle. Behavioral reactivity was evaluated as responsiveness to petting, intensity of dowel biting, and level of sonic vocalization when handled. Empty cage behaviors were scored by placing the mouse into a clean, empty cage and noting wild running, stereotypies, and excessive exploration levels.

Novel empty cage activity

Each subject was placed in a clean standard Tecniplast mouse cage and monitored for 1 hour. The cage bottom was covered with a thin layer of clean bedding, approximately 0.5 cm deep. The cage was covered with a metal wire bar lid and a plastic filter top. Food and water were not provided during the test session. Behaviors that occurred in the last 10 minutes of the 60-minute session were analyzed by time-sampling. An observation was taken every 30 seconds, and occurrence of circling, hanging on the wire lid, backflipping, self-grooming, resting, and/or exploration were recorded.

Open field exploration

Open field exploratory activities were evaluated as previously described (Silverman et al., 2011; Yang et al., 2012). Each animal was tested in a VersaMax Animal Activity Monitoring System (Accuscan, Columbus, OH) for a 10 min. session. Total distance traversed, horizontal activity, vertical activity, and time spent in the center were automatically recorded.

Acoustic startle response

Acoustic startle was measured using the SR-Laboratory System (San Diego Instruments, San Diego, CA) as described previously (Silverman et al., 2011; Yang et al., 2012). Test sessions began by placing the mouse in the Plexiglas holding cylinder for a 5-min. acclimation period. For the next 8 min., mice were presented with each of six trial types across six discrete blocks of trials, for a total of 36 trials. The inter-trial interval was 10–20 s. One trial type measured the response to no stimulus (baseline movement). The other five trial types measured startle responses to 40 ms sound bursts of 80, 90, 100, 110 or 120 dB. The six trial types were presented in pseudorandom order such that each trial type was presented once within a block of six trials. Startle amplitude of whole body flinch was measured every 1 ms over a 65 ms period beginning at the onset of the startle stimulus. The maximum startle amplitude over this sampling period was taken as the dependent variable. The background noise level of 70

dB was maintained over the duration of the test session.

Olfactory habituation/dishabituation test

The ability to smell non-social and social odors was tested as previously described (Silverman et al., 2011; Yang et al., 2012; Yang and Crawley, 2009). Each subject mouse was tested in a clean empty mouse cage containing a thin layer of fresh bedding, approximately 0.5 cm deep. Odor-saturated cotton-tipped swabs (6 in. length, Solon Manufacturing Company, Solon, Maine) were used to deliver odors. To reduce novelty-induced exploratory activities, each subject was habituated in the empty testing cage containing one clean dry cotton swab for 45 minutes before testing. The test consisted of fifteen 2-min trials: three trials with plain tap water, followed by three trials with of almond odor (prepared from almond extract, McCormick, Hunt Valley, MD; 1:100 dilution), three trials with banana odor (prepared from imitation banana flavor, McCormick, Hunt Valley, MD; 1:100 dilution), three trials with social odor from social cage 1, three trials with social odor from social cage 2. Water, almond odor, and banana odor stimuli were prepared by dipping the cotton tip briefly into the solution. Social odor stimuli were prepared by wiping a swab in a zig-zag motion across a soiled cage of unfamiliar mice of the same sex. For each subject, one soiled cage of 129/SvImJ mice and one soiled cage of C57BL/6J mice were the sources of the two social odors. Time spent sniffing the swab was recorded with a stopwatch by an observer sitting 2 meters away from the testing cage. Sniffing was scored when the nose was within 1 cm of the cotton swab. The inter-trial interval was approximately 1 minute.

Novel object recognition

The novel object recognition test was conducted as previously described (Brielmaier et al., 2012; Yang et al., 2012). Each animal was habituated to a clean empty Accuscan open field arena for 30 min., 24 hours before the experiment, and again for another 10 min. on the day of the experiment. After the second habituation session, the mouse was removed from the open field and placed in a clean temporary holding cage for approximately 2 min. Two identical objects were placed in the arena. Each subject was returned to the open field for a 10-min. familiarization session. The subjects were then removed from the open field, placed individually in a clean holding cage, and left undisturbed for an hour. For the recognition test, one clean familiar object and one

clean novel object were placed in the arena, and each subject was returned to its open field for a 5-min. recognition test. The recognition test sessions were videotaped and subsequently scored by two highly-trained investigators, uninformed of genotype, whose inter-rater reliability was $\geq 95\%$. Object investigation was defined as time spent sniffing the object when the nose was oriented toward the object and the nose-object distance was 2 cm or less. Recognition memory was defined as spending significantly more time sniffing the novel object than the familiar object. Total time spent sniffing both objects was used as a measure of general exploration.

Statistical analyses

One-Way ANOVA was used to detect genotype differences in pup body weight, body temperature, wire hang, juvenile social interactions, open field exploratory activity, and self-grooming. The Mann-Whitney U test was used to analyze novel home cage activity. Repeated Measures ANOVA was used to analyze rotarod motor learning, olfactory habituation/dishabituation, acoustic startle response, and novel object recognition. Time spent in the side chambers and time sniffing in three-chambered social test were analyzed by Repeated Measures ANOVA, with the factor of chamber side (novel mouse side vs. novel object side). Time spent in the center chamber appears in the graphs for illustrative purposes, but was not included in the statistical analysis.

Supplementary References

Antunes, M., and Biala, G. (2012). The novel object recognition memory: neurobiology, test procedure, and its modifications. *Cogn Process* 13, 93-110.

Avants, B.B., Tustison, N.J., Song, G., Cook, P.A., Klein, A., and Gee, J.C. (2011). A reproducible evaluation of ANTs similarity metric performance in brain image registration. *Neuroimage* 54, 2033-2044.

Bader, P.L., Faizi, M., Kim, L.H., Owen, S.F., Tadross, M.R., Alfa, R.W., Bett, G.C., Tsien, R.W., Rasmusson, R.L., and Shamloo, M. (2011). Mouse model of Timothy syndrome recapitulates triad of autistic traits. *Proc Natl Acad Sci U S A* 108, 15432-15437.

Bengtsson, M., Stahlberg, A., Rorsman, P., and Kubista, M. (2005). Gene expression profiling in single cells from the pancreatic islets of Langerhans reveals lognormal distribution of mRNA levels. *Genome Res* 15, 1388-1392.

Brielmaier, J., Matteson, P.G., Silverman, J.L., Senerth, J.M., Kelly, S., Genestine, M., Millonig, J.H., DiCicco-Bloom, E., and Crawley, J.N. (2012). Autism-relevant social abnormalities and cognitive deficits in engrailed-2 knockout mice. *PLoS One* 7, e40914.

Chadman, K.K., Gong, S., Scattoni, M.L., Boltuck, S.E., Gandhi, S.U., Heintz, N., and Crawley, J.N. (2008). Minimal aberrant behavioral phenotypes of neuroligin-3 R451C knockin mice. *Autism research : official journal of the International Society for Autism Research* 1, 147-158.

- Chubb, J.R., Trcek, T., Shenoy, S.M., and Singer, R.H. (2006). Transcriptional pulsing of a developmental gene. *Curr Biol* 16, 1018-1025.
- Collins, D.L., Neelin, P., Peters, T.M., and Evans, A.C. (1994). Automatic 3D intersubject registration of MR volumetric data in standardized Talairach space. *J Comput Assist Tomogr* 18, 192-205.
- Dorr, A.E., Lerch, J.P., Spring, S., Kabani, N., and Henkelman, R.M. (2008). High resolution three-dimensional brain atlas using an average magnetic resonance image of 40 adult C57Bl/6J mice. *Neuroimage* 42, 60-69.
- Ey, E., Yang, M., Katz, A.M., Woldeyohannes, L., Silverman, J.L., Leblond, C.S., Faure, P., Torquet, N., Le Sourd, A.M., Bourgeron, T., *et al.* (2012). Absence of deficits in social behaviors and ultrasonic vocalizations in later generations of mice lacking neuroligin4. *Genes Brain Behav*.
- Faizi, M., Bader, P.L., Saw, N., Nguyen, T.V., Beraki, S., Wyss-Coray, T., Longo, F.M., and Shamloo, M. (2012). Thy1-hAPP(Lond/Swe+) mouse model of Alzheimer's disease displays broad behavioral deficits in sensorimotor, cognitive and social function. *Brain Behav* 2, 142-154.
- Faizi, M., Bader, P.L., Tun, C., Encarnacion, A., Kleschevnikov, A., Belichenko, P., Saw, N., Priestley, M., Tsien, R.W., Mobley, W.C., *et al.* (2011). Comprehensive behavioral phenotyping of Ts65Dn mouse model of Down syndrome: activation of beta1-adrenergic receptor by xamoterol as a potential cognitive enhancer. *Neurobiol Dis* 43, 397-413.
- Genovese, C.R., Lazar, N.A., and Nichols, T. (2002). Thresholding of statistical maps in functional neuroimaging using the false discovery rate. *Neuroimage* 15, 870-878.
- Ishizaki, T., Erickson, A., Kuric, E., Shamloo, M., Hara-Nishimura, I., Inacio, A.R., Wieloch, T., and Ruscher, K. (2010). The asparaginyl endopeptidase legumain after experimental stroke. *J Cereb Blood Flow Metab* 30, 1756-1766.
- Kern, A., Albarran-Zeckler, R., Walsh, H.E., and Smith, R.G. (2012). Apo-ghrelin receptor forms heteromers with DRD2 in hypothalamic neurons and is essential for anorexigenic effects of DRD2 agonism. *Neuron* 73, 317-332.
- Lau, J.C., Lerch, J.P., Sled, J.G., Henkelman, R.M., Evans, A.C., and Bedell, B.J. (2008). Longitudinal neuroanatomical changes determined by deformation-based morphometry in a mouse model of Alzheimer's disease. *Neuroimage* 42, 19-27.
- Nieman, B.J., Flenniken, A.M., Adamson, S.L., Henkelman, R.M., and Sled, J.G. (2006). Anatomical phenotyping in the brain and skull of a mutant mouse by magnetic resonance imaging and computed tomography. *Physiol Genomics* 24, 154-162.
- Nieman, B.J., Lerch, J.P., Bock, N.A., Chen, X.J., Sled, J.G., and Henkelman, R.M. (2007). Mouse behavioral mutants have neuroimaging abnormalities. *Hum Brain Mapp* 28, 567-575.
- Raj, A., Peskin, C.S., Tranchina, D., Vargas, D.Y., and Tyagi, S. (2006). Stochastic mRNA synthesis in mammalian cells. *PLoS Biol* 4, e309.
- Scattoni, M.L., Gandhi, S.U., Ricceri, L., and Crawley, J.N. (2008). Unusual repertoire of vocalizations in the BTBR T+tf/J mouse model of autism. *PLoS One* 3, e3067.
- Silverman, J.L., Turner, S.M., Barkan, C.L., Tolu, S.S., Saxena, R., Hung, A.Y., Sheng, M., and Crawley, J.N. (2011). Sociability and motor functions in Shank1 mutant mice. *Brain Res* 1380, 120-137.
- Suter, D.M., Molina, N., Gatfield, D., Schneider, K., Schibler, U., and Naef, F. (2011). Mammalian genes are transcribed with widely different bursting kinetics. *Science* 332, 472-474.
- Tang, S.H., Silva, F.J., Tsark, W.M., and Mann, J.R. (2002). A Cre/loxP-deleter transgenic line in mouse strain 129S1/SvImJ. *Genesis* 32, 199-202.
- Weiss, L.A., Shen, Y., Korn, J.M., Arking, D.E., Miller, D.T., Fossdal, R., Saemundsen, E., Stefansson, H., Ferreira, M.A., Green, T., *et al.* (2008). Association between microdeletion and microduplication at 16p11.2 and autism. *N Engl J Med* 358, 667-675.

Yang, M., Bozdagi, O., Scattoni, M.L., Wohr, M., Roullet, F.I., Katz, A.M., Abrams, D.N., Kalikhman, D., Simon, H., Woldeyohannes, L., *et al.* (2012). Reduced excitatory neurotransmission and mild autism-relevant phenotypes in adolescent Shank3 null mutant mice. *J Neurosci* 32, 6525-6541.

Yang, M., and Crawley, J.N. (2009). Simple behavioral assessment of mouse olfaction. *Current protocols in neuroscience / editorial board, Jacqueline N Crawley [et al] Chapter 8, Unit 8 24.*

Yang, M., Silverman, J.L., and Crawley, J.N. (2011). Automated three-chambered social approach task for mice. *Current protocols in neuroscience / editorial board, Jacqueline N Crawley [et al] Chapter 8, Unit 8 26.*